4. Conclusions

Pedestal temperature models that include the effects of both first and second stability of ballooning modes are developed for type I ELMy H-mode plasmas in tokamaks. The results for the pedestal temperature, width and pressure gradient are compared with high resolution data points in the ITPA Pedestal Database version 3.2. It is found that the inclusion of the second stability of ballooning modes improves the agreement with experimental data for the pedestal pressure gradient and, consequently, for the width. The predictions of ion and electron pedestal temperatures for ITER using these models are carried out. It is found that at the design point assuming a flat density profile, the pedestal temperature of ITER can reach 2.3 keV.

5. Acknowledgements

T. Onjun is grateful to Prof. Suthat Yoksan for his helpful discussions and also thanks the ITPA Pedestal Database group for the pedestal data used in this work. This work is supported by Commission on Higher Education and the Thailand Research Fund (TRF) under Contract No. MRG4880165.

6. Referecnes

[1] Kinsey J.E., Bateman G., Onjun T., *et al.*, Burning plasma projections using drift-wave transport models and scalings for the H-mode pedestal, Nucl. Fusion, Vol. 43, pp. 1845, 2003

[2] Aymar, R., Barabaschi, P. and Shimomura, Y. (for the ITER team), The ITER design, Plasma Phys. Control. Fusion, Vol. 44, pp. 519, 2002

[3] Onjun, T., Bateman, G., Kritz, A.H. and Hammett G., Models for the pedestal temperature at the edge of H-mode tokamak plasmas, Physics of Plasmas, Vol. 9, pp. 5018. 2002

[4] Sugihara, M., Igitkhanov, Yu., Janeschitz, G., *et al.*, A model for H-mode pedestal width scaling using the International Pedestal Database, Nuclear Fusion, Vol. 40, pp. 1743, 2000

[5] Osborne, T.H., Burrell, K.H., Groebner, R.J., *et al.*, H-mode pedestal characteristics in ITER shape discharges on DIII-D, Journal of Nuclear Materials, Vol. 266-269, pp. 131, 1999

[6] Wesson, J., Tokamaks, Clarendon Oxford England, 1997

[7] Kamada, Y., Hatae, T., Fukuda, T., *et al.*, Growth of the edge pedestal in JT-60U ELMy H-mode, Plasma Phys. Control. Fusion, Vol. 41, pp. 1371, 1999

[8] Osborne, T.H., Ferron, J.R., Groebner, R.J., *et al.*, The effect of plasma shape on H-mode pedestal characteristics on DIII-D, Plasma Phys. Control. Fusion, Vol. 42, pp. A175, 2000

[9] Suttrop, W., Gruber, O., Kurzan, B., *et al.*, Effect of plasma shape variation on ELMs and H-mode pedestal properties in ASDEX Upgrade, Plasma Phys. Control. Fusion, Vol. 42, pp. A97, 2000

[10] Onjun, T., Kritz, A., Bateman, G., *et al.*, Stability analysis of H-mode pedestal and edge localized modes in a Joint European Torus power scan, Physics of Plasmas, Vol. 11, pp. 1469, 2004
[11] Onjun, T., Kritz, A.H., Bateman, G., *et al.*, Integrated pedestal and core modeling of Joint European Torus (JET) triangularity scan discharges, Phys. Plasmas, Vol. 11, pp. 3006, 2004
[12] Lönnroth, J-S., Parail, V. V., Corrigan, G., et al., Integrated predictive modelling of the effect of neutralgas puffing in ELMy H-mode plasmas, Plasma Phys. Control. Fusion, Vol. 45, pp. 1689, 2003
[13] Hatae, T., Sugihara, M., Hubbard, A.E., *et al.*, Understanding of H mode pedestal characteristics using the multimachine pedestal database, Nucl. Fusion, Vol. 41, pp. 285, 2001

Table 1: Coefficients and RMSEs of the models using the normalized pressure gradient model including both first and second stability limits of ballooning modes.

Width scaling	C_w	C_0	RMSE_T_{ped} (%)	RMSE_Δ (%)	RMSE_dp/dr (%)
$\Delta\propto(\rho Rq)^{1/2}$	0.10	0.8	60	32	56
$\Delta\propto\rho s^2$	0.29	0.8	63	38	51
$\Delta\propto(\beta_{\theta,ped})^{1/2}$	0.012	0.8	57	30	54

Table 2: Coefficients and RMSEs of the models using the normalized pressure gradient model including only first stability limits of ballooning modes.

Width scaling	C_w	RMSE_T_{ped} (%)	RMSE_Δ (%)	RMSE_dp/dr (%)
$\Delta\propto(\rho Rq)^{1/2}$	0.22	57	76	95
$\Delta\propto\rho s^2$	2.41	64	87	96
$\Delta\propto(\beta_{\theta,ped})^{1/2}$	0.021	62	43	81

Table 3: RMSEs of the electron pedestal temperature models using the normalized pressure gradient model including both first and second stability limits of ballooning modes when applied to the full pedestal database.

Width scaling	C_0	Electron pedestal temperature		Ion pedestal temperature	
		C_w	RMSE_T_{ped} (%)	C_w	RMSE_T_{ped} (%)
$\Delta\propto(\rho Rq)^{1/2}$	0.8	0.10	44	0.094	30
$\Delta\propto\rho s^2$	0.8	0.29	37	0.41	31
$\Delta\propto(\beta_{\theta,ped})^{1/2}$	0.8	0.012	167	0.0082	34

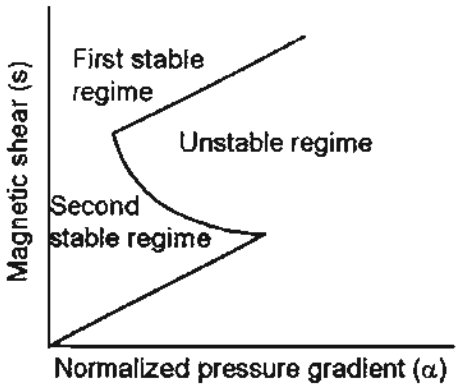

Figure 1: The normalized pressure gradient vs. magnetic shear diagram (s-α diagram) is plotted. First and second stability region and unstable region is also described.

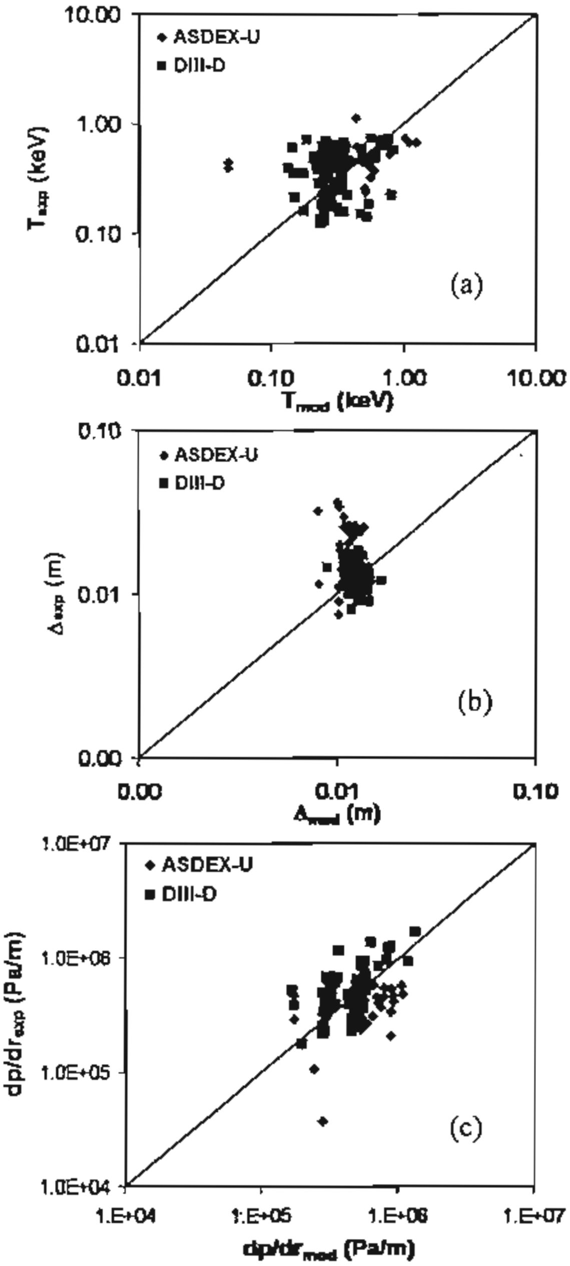

Figure 2: Plot for the pedestal temperature (a), width (b), and pressure gradient (c) predicted by model based on $\Delta \propto \rho s^2$ and the pedestal pressure gradient including both first and second stability of ballooning mode compared with experimental data from 124 data points. Each tokamak is indicated by a different symbol.

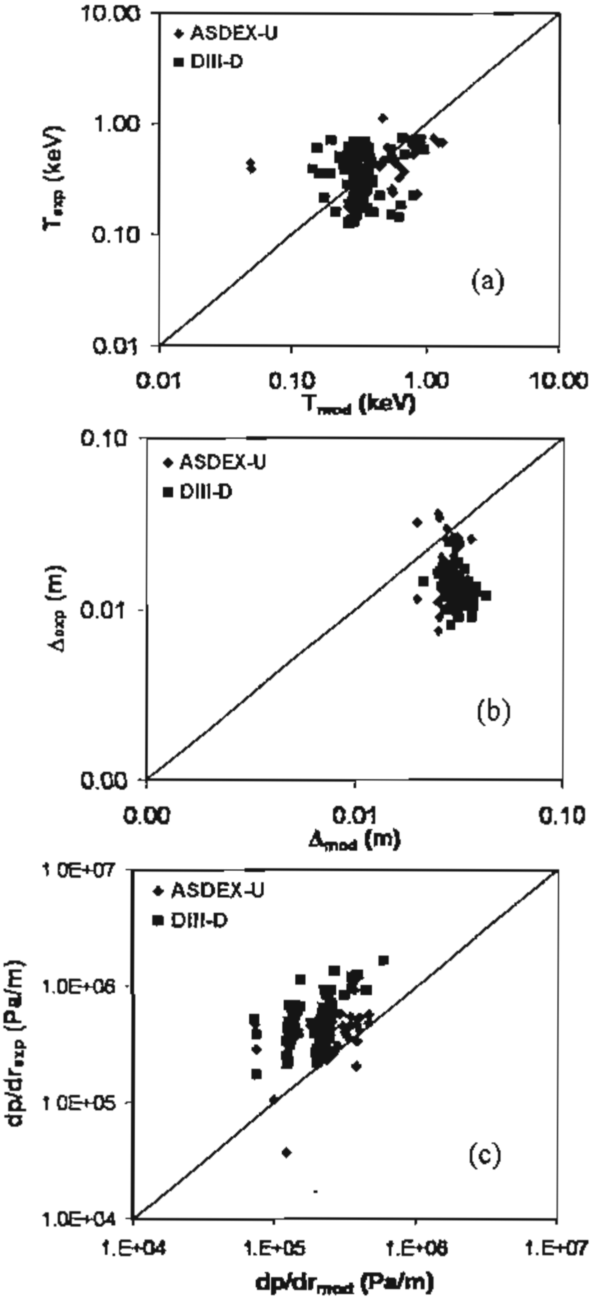

Figure 3: Plot for the pedestal temperature (a), width (b), and pressure gradient (c) predicted by model based on $\Delta \propto \rho s^2$ and the pedestal pressure gradient including only first stability compared with experimental data from 124 data points.

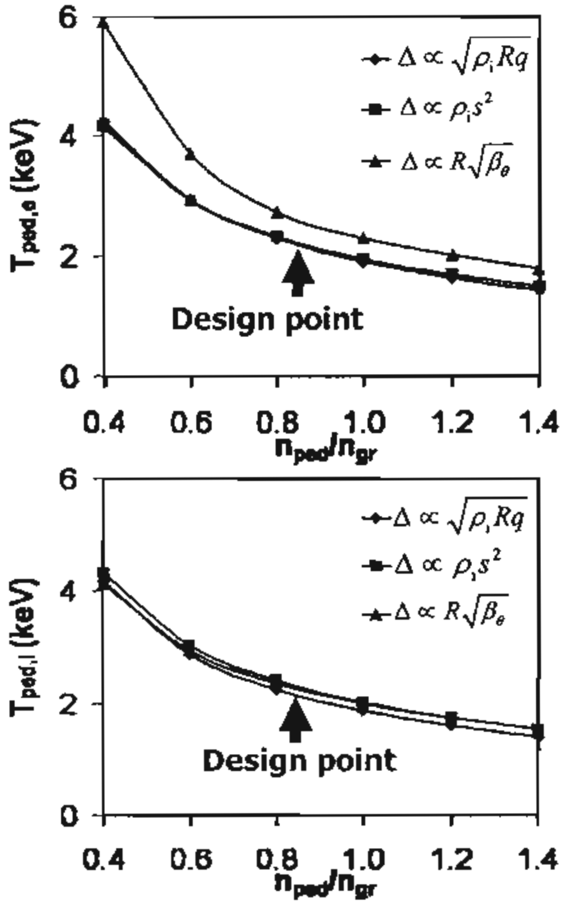

Figure 4: Predictions of electron (top) and ion (bottom) pedestal temperature as a function of the pedestal density based on three pedestal temperature models.

Second Ballooning Stability Effect on H-mode Pedestal Scalings

T. Onjun 1), A.H. Kritz 2), G. Bateman 2), A. Pankin 2)

1) Sirindhorn International Institute of Technology, Klong Luang, Pathumthani, Thailand
2) Department of Physics, Lehigh University, Pennsylvania, USA

E-mail: thawatchai@siit.tu.ac.th

Abstract. Models for the prediction of ion and electron pedestal temperatures at the edge of type I ELMy H-mode plasmas are developed. These models are based on theory motivated concepts for pedestal width and pressure gradient. The pedestal pressure gradient is assumed to be limited by high n ballooning mode instabilities, where both the first and second stability limits are considered. The effect of the bootstrap current, which reduces the magnetic shear in the steep pressure gradient region at the edge of the H-mode plasma, can result in access to the second stability of ballooning mode. In these pedestal models, the magnetic shear and safety factor are calculated at a radius that is one pedestal width away from separatrix. The predictions of these models are compared with pedestal data for type I ELMy H-mode discharges obtained from the latest public version (version 3.2) in the International Tokamak Physics Activity Edge (ITPA) Pedestal Database. It is found that the pedestal temperature model based on the magnetic and flow shear stabilization yields the best agreement with experimental data (RMSE of 28.2%). For standard H-mode ITER discharges with 15 MA plasma current, predictive analysis yields ion and electron temperatures at the top of the H-mode pedestal in the range from 1.7 to 1.9 keV.

1. Introduction

It is well known that when the plasma heating power increases, plasmas can undergo a spontaneous self-organizing transition from a low confinement mode (L-mode) to a high confinement mode (H-mode). This plasma activity is widely believed to be caused by the generation of a flow shear at the edge of plasma, which is responsible for suppressed turbulence and transport near the edge of plasma. The reduction of transport near the plasma edge results in a narrow sharply-defined region at the edge of the plasma with steep temperature and density gradients, called the pedestal. This pedestal is located near the last closed magnetic flux surface and typically extends over with a width of about 5% of the plasma minor radius. It was found that energy confinement in the H-mode regime of tokamaks strongly depends on the temperature and density at the top of the pedestal [1]. Therefore, it is important in H-mode tokamak plasma studies, especially for the burning plasma experiment such as the International Thermonuclear Experimental Reactor (ITER) [2], to have a reliable prediction for temperatures at the top of the pedestal.

In the previous pedestal study by T. Onjun *et al.* [3], six theory-based pedestal temperature models were developed using different models for the pedestal width together with a ballooning mode pressure gradient limit that is restricted to the first stability of ballooning modes. These models also include the effects of geometry, bootstrap current, and separatrix, leading to a complicated nonlinear behavior. For the best model, the agreement between model's predictions and experimental data for pedestal temperature is about 30.8% RMSE for 533 data points from the International Tokamak Physics Activity Edge (ITPA) Pedestal Database. One weakness of these pedestal temperature models is the assumption that the plasma pedestal is in the first stability regime of ballooning modes.

In this study, six pedestal width models in Refs. [3-8] are modified to include the effect of the second stability limit of ballooning modes. The predictions from these pedestal temperature models are be tested against the latest public version of the pedestal data (Version 3.2) obtained from the ITPA Pedestal Database. This paper is organized in the following way: In Section 2, the pedestal temperature model development is described. In Section 3, the predictions of the pedestal temperature resulting from the models are compared with pedestal temperature experimental data. A simple statistical analysis is used to characterize the agreement of the predictions of each model with experimental data. The development and comparison with experimental data for the pedestal density models are shown in Section 4. In Section 5, conclusions are presented

2. H-Mode Pedestal Temperature Model

Each pedestal temperature model described in Ref. [1] has two parts: a model for the pedestal width (Δ) and a model for the pressure gradient ($\partial p/\partial r$). The pedestal density, $n_{\rm ped}$, is obtained directly from the experiment or from the pedestal density model described in Section 4. The temperature at the top of the pedestal ($T_{\rm ped}$) can be estimated as

$$T_{\rm ped} = \frac{1}{2\, n_{\rm ped}\, k} \left| \frac{\partial p}{\partial r} \right| \Delta \qquad (1)$$

where k is the Boltzmann constant. Six pedestal models were developed based on Eq. (1) in Ref. [3]. These pedestal models are based on (1) the flow shear stabilization width model [$\Delta \propto (\rho R q)^{1/2}$] [3], (2) the magnetic and flow shear stabilization width model [$\Delta \propto \rho s^2$] [4], (3) the normalized poloidal pressure width model [$\Delta \propto R(\beta_{\theta,\rm ped})^{1/2}$] [5], (4) the diamagnetic stabilization width model [$\Delta \propto \rho^{2/3} R^{1/3}$] [6], (5) the ion orbit loss width model [$\Delta \propto \varepsilon^{1/2} \rho_\theta$] [7], and (6) the two fluid Hall equilibrium width model [$\Delta \propto (1/Z)(A_{\rm H}/n_{\rm ped})^{1/2}$] [8]. Note that the constant of proportionality in the pedestal width scaling based the two fluid Hall equilibrium width model in Ref. [8] is varied in this work to improve agreement with experimental data. These six pedestal width models are used in this paper together with an improved pressure gradient model to develop new pedestal temperature models.

For the maximum pressure gradient in the pedestal of type I ELMy H-mode discharges, the pedestal pressure gradient is approximated as the pressure gradient limit of high-n ballooning modes in the short toroidal wavelength limit. The ballooning mode is usually described using the magnetic shear vs. normalized pressure gradient diagram (s-α diagram). Normally, the calculation of ballooning mode stability is complicated, requiring information about the plasma equilibrium and geometry. A number of different codes have been developed for stability analysis, such as HELENA, MISHKA and ELITE. In Ref. [9], stability analyses for JET triangularity scan H-mode discharges were carried out using the HELENA and MISHKA ideal MHD stability codes. For the JET high triangularity discharge 53298, the stability analysis results are shown in fig. 10 in Ref. [9]. Based on results obtained in Ref. [9], the s-α MHD stability diagram with both the first and second stability effects included can be simplified as Fig. 1. This s-α MHD stability diagram leads to an analytic expression for the critical normalized pressure gradient α_c that includes the effect of both the first and second stability of ballooning modes and geometrical effects given by:

$$\alpha_c \equiv -\frac{2\mu_0 R q^2}{B_T^2}\left(\frac{dp}{dr}\right)_c = \alpha_0(s)\left[\frac{1+\kappa_{95}^2\left(1+10\delta_{95}^2\right)}{7}\right]. \tag{2}$$

where μ_0 is the permeability of free space, R is the major radius, q is the safety factor, B_T is the toroidal magnetic field, s is the magnetic shear, κ_{95} and δ_{95} are the elongation and triangularity at the 95% flux surface, and $\alpha_0(s)$ is a function of magnetic shear as

$$\alpha_0(s) = \begin{cases} 3+0.8(s-4) & s>6 \\ 6-3\sqrt{1-\left(\frac{6-s}{3}\right)^2} & 6\geq s\geq 3. \\ 6 & 3>s \end{cases} \tag{3}$$

Note that in this work, the effect of geometry on the plasma edge stability has a similar form with that used in Ref. [3], but somewhat stronger. The function in Eq. (3) can be understood as the following: for $s > 6$, the equation indicates that the pedestal is in the first stability regime of ballooning modes; for $6 \geq s \geq 3$, the equation represents the regime of a transition from first to second stability of ballooning modes; for $s < 3$, the equation represents a plasma that is in the second stability of ballooning modes, where the pedestal pressure gradient is limited by finite n ballooning mode stability. It should be noted that the effect of the current-driven peeling mode is not considered in this work. In Eq. (3), the bootstrap current and separatrix effects are included through the calculation of magnetic shear as described in Ref. [1]. Note that the magnetic shear in Ref. [3] is calculated as

$$s = s_0\left(1-\frac{c_{bs}b(\upsilon^*,\varepsilon)\alpha_c}{4\sqrt{\varepsilon}}\right), \tag{4}$$

where the multiplier C_{bs} is adjusted to account for the uncertainty of the bootstrap current effect.

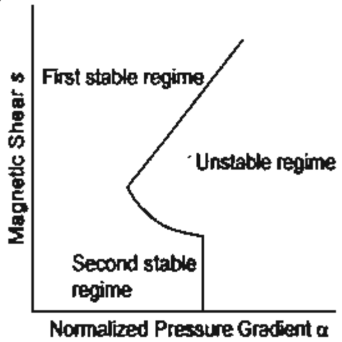

Fig. 1: The normalized pressure gradient vs. magnetic shear diagram (s-α diagram) is plotted. First and second stability region and unstable region is also described.

3. Results and Discussions

Statistical comparisons between predicted pedestal parameters and corresponding experimental values obtained from the ITPA Pedestal Database [10] version 3.2 are carried out. To quantify the comparison between the predictions of each model and experimental data, the root mean-square error (RMSE), the offset, and the Pearson product moment correlation coefficient (R) are computed. The RMSE, offset, and correlation R are defined as

$$\mathrm{RMSE}\ (\%) = 100 \times \sqrt{\frac{1}{N}\sum_{j=1}^{N}\left[\ln\left(T_j^{\exp}\right) - \ln\left(T_j^{\mathrm{mod}}\right)\right]^2}\ ,$$

$$\mathrm{Offset}(\%) = \frac{100}{N}\sum_{j=1}^{N}\left[\ln\left(T_j^{\exp}\right) - \ln\left(T_j^{\mathrm{mod}}\right)\right],$$

$$R = \frac{\sum_{j=1}^{N}\left(\ln\left(T_j^{\exp}\right) - \overline{\ln\left(T_j^{\exp}\right)}\right)\left(\ln\left(T_j^{\mathrm{mod}}\right) - \overline{\ln\left(T_j^{\mathrm{mod}}\right)}\right)}{\sqrt{\sum_{j=1}^{N}\left(\ln\left(T_j^{\exp}\right) - \overline{\ln\left(T_j^{\exp}\right)}\right)^2\left(\ln\left(T_j^{\mathrm{mod}}\right) - \overline{\ln\left(T_j^{\mathrm{mod}}\right)}\right)^2}}$$

where N is total number of data points, and $T_j^{\exp}$ and T_j^{mod} are the j^{th} experimental and model results for the temperature.

Six scalings for the pedestal temperature are derived using the six models described above for the width of the pedestal together with the model given by Eqs. (2) and (3) for the critical pressure gradient that includes both the first and second stability of ballooning modes. The pedestal temperature scalings are calibrated using 457 experimental data points (90 from JET experiment, and 367 from JT-60U experiment) for the ion pedestal temperature from the ITPA Pedestal Database (Version 3.2). The statistical results are shown in Table 1. The value of the coefficient, C_w, used in each of the expressions for the pedestal width and the value of multiplier C_{bs} used in the calculation of magnetic shear are given in the second and third column of Table 1, respectively. It is found that the RMSEs for the pedestal temperature range from 28.2% to 109.4%, where the model based on $\Delta \propto \rho s^2$ yields the lowest RMSE. For the offset, it is shown in Table 1 that the offsets range from -6.5% to 9.0%, where the model based on $\Delta \propto \rho s^2$ yields the best agreement (smallest absolute value of the offset). For the correlation R, it is shown in Table 1 that the values of correlation R range from 0.28 to 0.80, where the model based on $\Delta \propto \rho s^2$ yields the best agreement (highest value of R). From these results, it can be concluded that the pedestal temperature based on $\Delta \propto \rho s^2$ yields the best average agreement with experimental data.

Table 1: Statistical results of the models for type 1 ELMy H-mode discharges.

Pedestal width scaling	C_w	C_{bs}	RMSE (%)	Offset (%)	R
$\Delta \propto \rho s^2$	5.10	3.0	28.2	0.5	0.80
$\Delta \propto (\rho R q)^{1/2}$	0.22	4.5	35.4	2.9	0.75
$\Delta \propto R(\beta_{\theta,\mathrm{ped}})^{1/2}$	1.50	3.7	35.5	-1.0	0.73
$\Delta \propto \rho^{2/3} R^{1/3}$	1.37	4.9	49.3	-1.1	0.67
$\Delta \propto \varepsilon^{1/2} \rho_\theta$	2.75	4.9	109.4	9.0	0.28
$\Delta \propto (1/Z)(A_H/n_{\mathrm{ped}})^{1/2}$	0.014	5.9	50.5	-6.5	0.68

The comparisons between the predictions of the models and experimental data are shown in Figs. 2-7. It can be seen that the predictions of pedestal temperature are in reasonable agreement with experimental data for the model with $\Delta \propto \rho s^2$ shown in Fig. 2 and the agreement is not as good for the other models shown in Figs. 3-7.

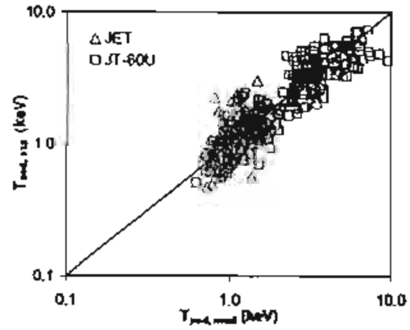

Fig. 2: Experimental ion pedestal temperature for type I H-mode plasmas compared with the model predictions based on $\Delta \propto \rho s^2$.

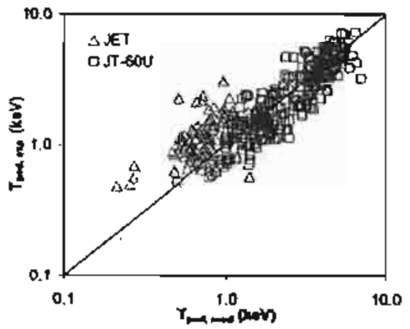

Fig. 3: Experimental ion pedestal temperature for type I H-mode plasmas compared with the model predictions based on $\Delta \propto (\rho R q)^{1/2}$.

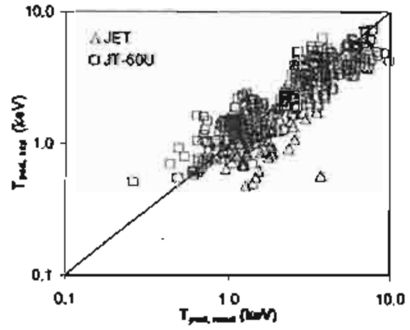

Fig. 4: Experimental ion pedestal temperature for type I H-mode plasmas compared with the model predictions based on $\Delta \propto R(\beta_{\theta,\mathrm{ped}})^{1/2}$.

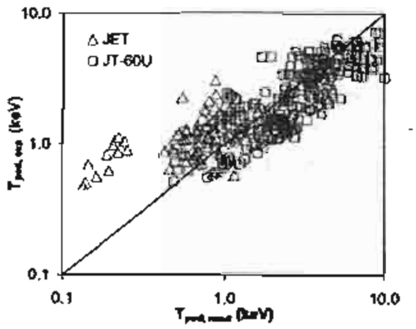

Fig. 5: Experimental ion pedestal temperature for type I H-mode plasmas compared with the model predictions based on $\Delta \propto \rho^{2/3} R^{1/3}$.

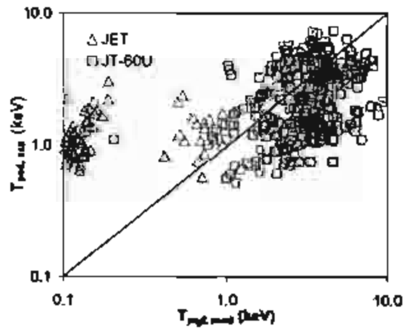

Fig. 6: Experimental ion pedestal temperature for type I H-mode plasmas compared with the model predictions based on $\Delta \propto \varepsilon^{1/2} \rho_\theta$.

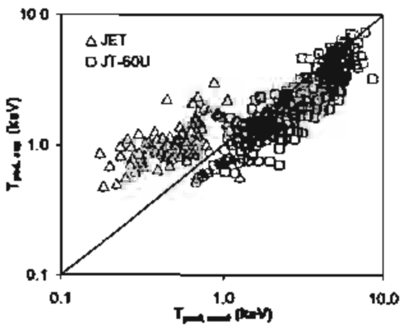

Fig. 7: Experimental ion pedestal temperature for type I H-mode plasmas compared with the model predictions based on $\Delta \propto (1/Z)(A_H/n_{\mathrm{ped}})^{1/2}$.

4. H-Mode Pedestal Density Model

In the, development of the pedestal density model, an empirical approach is employed. For the simplest scaling, the pedestal density is assumed to be a function of line average density (n_l). This assumption is based on an observation that the density profile between the pedestal and the magnetic axis in H-mode discharges is usually rather flat. Therefore, the pedestal density is a large fraction of the line average density. It is found that the pedestal density scaling for type I ELMy H-mode discharges is about 72% of the line average density, which can be described as

$$n_{ped} = 0.72 n_l \,. \tag{5}$$

This scaling yields an RMSE of 12.2%, R^2 of 0.96, and offset of -2.2% with a data set of 626 data points (132 from ASDEX-U experiment, 127 from JET experiment, and 367 from JT-60U experiment). In Ref. [11], a pedestal density scaling is developed. for Alcator CMOD H-mode discharges. This scaling is expressed as a function of the line average density, plasma current (I_p), and toroidal magnetic field (B_T). Using this kind of power law regression fit for the 626 data points in the ITPA Pedestal Database (Version 3.2), the best predictive pedestal density scaling for type I ELMy H-mode discharges is found to be

$$n_{ped}\left[10^{20}\text{m}^{-3}\right] = 0.74\left(n_l\left[10^{20}\text{m}^{-3}\right]\right)^{0.99}\left(I_p\left[MA\right]\right)^{0.15}\left(B_T\left[T\right]\right)^{-0.12} . \tag{6}$$

This scaling yields an RMSE of 10.9%, R^2 of 0.97, and offset of 3.3%. The comparisons of the density models' predictions for the pedestal density using Eq. (5) and (6) and the experimental data are shown in Figs. 8 and 9, respectively. In both figures, the agreement is good for a low ratio of pedestal density to the Greenwald density. However, the agreement tends to break-away at high density. This might indicate that the physics that controls low and high edge density might be different.

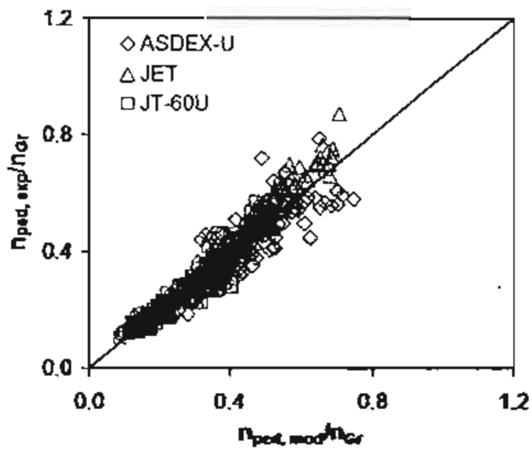

Fig. 8: The ratios of experimental pedestal electron density for type I H-mode plasmas to the Greenwald density are compared with the ratio of the model predictions using Eq. (5) to the Greenwald density.

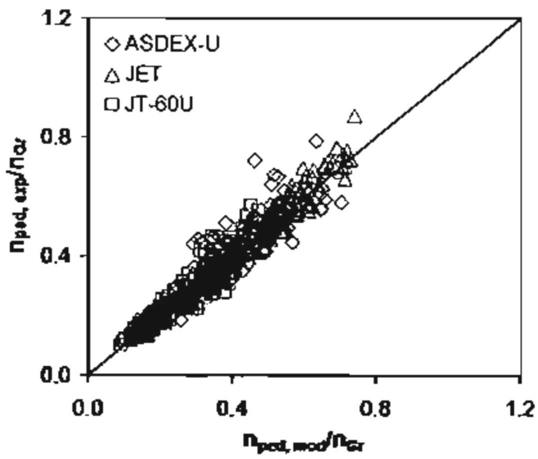

Fig. 9: The ratios of experimental pedestal electron density for type I H-mode plasmas to the Greenwald density are compared with the ratio of the model predictions using Eq. (6) to the Greenwald density.

5. Pedestal Prediction in ITER

The pedestal temperature and density models developed in this paper are used to predict the pedestal parameters for the ITER design. For an ITER standard H-mode discharge with 15 MA plasma current and the line average density of 1.05×10^{20} particles/m^3, the pedestal density is predicted to be 0.76×10^{20} particles/m^3 and 0.95×10^{20} particles/m^3 using Eqs. (5) and (6), respectively. It is worth noting that the pedestal density using Eq.(6) indicate a flat density profile since the pedestal density is almost the same as the line average density. This observation is often observed in H-mode experiments with high density. In addition, the pedestal density in ITER predicted using an integrated modeling code JETTO yields similar result for the density profile [12]. The pedestal temperature model based on the width of the pedestal as $\Delta \propto \rho s^2$ and the critical pressure gradient model that includes both first and second stability of ballooning modes is used to predict the pedestal temperature in ITER. Figure 10 shows the predicted pedestal temperature as a function of pedestal density. It can be seen that the pedestal temperature decreases as the pedestal density increases. At the predicted pedestal density using Eqs. (5) and (6), the predicted pedestal temperature is 1.9 and 1.7, respectively. Under these conditions, it is found that the pedestal width in ITER predicted by the model ranges from 4 to 5 cm.

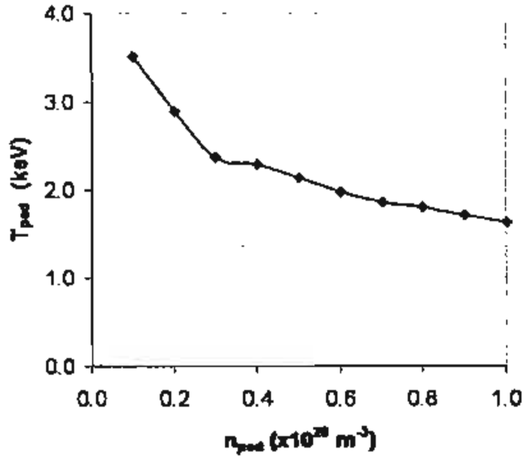

Fig. 10: Predictions of pedestal temperature as a function of pedestal density using the pedestal temperature model based on $\Delta \propto \rho s^2$

6. Conclusions

Pedestal temperature models that include the effects of both the first and second stability of ballooning modes are developed for type I ELMy H-mode plasmas in tokamaks. The results for the pedestal temperature are compared with experimental data obtained from the ITPA Pedestal Database version 3.2. It is found that the pedestal temperature model based on the magnetic and flow shear stabilization yields the best agreement with experimental data (with RMSE of 28.2%). It is found that the predictions of pedestal temperatures for ITER using the pedestal temperature and density models developed ranges from 1.7 to 1.9 keV.

4. Acknowleagement

Authors are grateful to Prof. Suthat Yoksan for his helpful discussions and to the ITPA Pedestal Database group for the pedestal data used in this work. This work is partially supported by Commission on Higher Education and the Thailand Research Fund (TRF) under Contract No. MRG4880165.

5. Referecnes

[1] Kinsey J E *et al.*, 2003 *Nucl. Fusion* **43** 1845
[2] Aymar R *et al.*, 2002 *Plasma Phys. Control. Fusion* **44** 519
[3] Onjun T *et al.*, 2002 *Phys. Plasmas* **9** 5018
[4] M Sugihara *et al.*, 2000 *Nucl. Fusion* **40** 1743
[5] T H Osborne *et al.*, 1999 *J. Nucl. Mater.* **266–269** 131
[6] B N Rogers *et al.*, 1999 *Phys. Plasmas* **6** 2797
[7] K C Shaing, 1992 *Phys. Fluids B* **4** 290
[8] Guzdar P N *et al.*, 2005 *Physics of Plasmas* **12** 032502
[9] Onjun T *et al.*, 2004 *Phys. Plasmas* **11** 3006
[10] Hatae T *et al.*, 2001 *Nucl. Fusion* **41** 285
[11] Hughes J W *et al.*, 2002 *Physics of Plasmas* **9** 3019
[12] Onjun T *et al.*, 2005 *Physics of Plasmas* **12** 082513

บทความทางวิชาการที่ส่งตีพิมพ์ในวารสารวิชาการ Laser and Particle Beams

The study of second ballooning stability effect on H-mode pedestal scalings

Thawatchai Onjun
Sirindhorn International Institute of Technology, Thammasat University,
Klong Luang, Pathumthani, Thailand
E-mail: thawatchai@siit.tu.ac.th

Abstract

Models for the prediction of ion pedestal temperature at the edge of type I ELMy H-mode plasmas are developed. These models are based on theory motivated concepts for pedestal width and pressure gradient. The pedestal pressure gradient is assumed to be limited by high *n* ballooning mode instabilities, where both the first and second stability limits are considered. The effect of the bootstrap current, which reduces the magnetic shear in the steep pressure gradient region at the edge of the H-mode plasma, can result in access to the second stability of ballooning mode. In these pedestal models, the magnetic shear and safety factor are calculated at a radius that is one pedestal width away from separatrix. The predictions of these models are compared with pedestal data for type I ELMy H-mode discharges obtained from the latest public version (version 3.2) in the International Tokamak Physics Activity Edge (ITPA) Pedestal Database. It is found that the pedestal temperature model based on the magnetic and flow shear stabilization yields the best agreement with experimental data (RMSE of 28.2%). For standard H-mode ITER discharges with 15 MA plasma current, predictive analysis yields ion and electron temperatures at the top of the H-mode pedestal is 1.7 keV.

Keywords: Tokamak, H-mode, Pedestal, Stability

1. Introduction

It has been widely accepted that at this moment, there are two leading candidates to harvest the energy from nuclear fusion reactions: Magnetic confinement fusion and inertial confinement fusion. While in inertial fusion the discussion for the most appropriate way to ignite a fusion pellet is still going on and is concerned with instabilities (Deutsch *et al.*, 2005), and the interaction of charge particle and laser beams with dense plasma (Deutsch 2004; Mulser *et al.*, 2004), the underlying nuclear physics is similar for both approaches (Hora 2004; Li *et al.*, 2004). With the decision to construct "the International Thermonuclear Experimental Reactor (ITER)" (Aymar *et al.*, 2002) in France, a big step forward has been taken to explore the properties of long burning plasma. In this paper, we address one of crucial issues of the magnetic confinement fusion, especially for the future burning plasma experiment such as ITER. Since the height of the pedestal strongly influences the plasma performance in the high confinement mode (H-mode) operation of the magnetic confinement fusion (Greenwald *et al.*, 1997), it is important to understand the physics that governs the H-mode pedestal.

When the plasma heating power increases, plasmas can undergo a spontaneous self-organizing transition from a low confinement mode (L-mode) to a high confinement mode (H-mode). This plasma activity is widely believed to be caused by the generation of a flow shear at the edge of plasma, which is responsible for suppressed turbulence and transport near the edge of plasma. The reduction of transport near the plasma edge results in a narrow sharply-defined region at the edge of the plasma with steep temperature and density gradients, called the pedestal. This pedestal is located near the last closed magnetic flux surface and typically extends over with a width of about 5% of the plasma minor radius. It was found that energy confinement in the H-mode regime of tokamaks strongly depends on the temperature and density at the top of the pedestal (Kinsey *et al.*, 2003). Therefore, it is important in H-mode tokamak plasma studies, especially for the burning plasma experiment such as ITER, to have a reliable prediction for temperatures at the top of the pedestal.

In the previous pedestal study by T. Onjun and his co-workers (Onjun *et al.*, 2002), six theory-based pedestal temperature models were developed using different models for the pedestal width together with a ballooning mode pressure gradient limit that is restricted to the first stability of ballooning modes. These models also include the effects of geometry, bootstrap current, and separatrix, leading to a complicated nonlinear behavior. For the best model, the agreement between model's predictions and experimental data for pedestal temperature is about 30.8% RMSE for 533 data points from the International Tokamak Physics Activity Edge (ITPA) Pedestal Database. One weakness of these pedestal temperature models is the assumption that the plasma pedestal is in the first stability regime of ballooning modes. In the recent pedestal modeling by T. Onjun (Onjun 2006), the pedestal model is extended to include the second stability effect of ballooning modes using a simple scaling. It was found that it can improve the agreement between the prediction and experimental data.

In this study, six pedestal width models used in the previous pedestal study by T. Onjun and his co-workers (Onjun *et al.*, 2002) are modified to include the effect of the second stability limit of ballooning modes, where the model for the stability limit of ballooning modes is based on stability analysis results from the HELENA and MISKHA stability analysis codes. The predictions from these pedestal temperature models are be tested against the latest public version of the pedestal data (Version 3.2) obtained from the ITPA Pedestal Database. This paper is organized in the following way: In Section 2, the pedestal temperature model development is described. In Section 3, the predictions of the pedestal temperature resulting from the models are compared with pedestal temperature experimental data. A simple statistical analysis is used to characterize the agreement of the predictions of each model with experimental data. The development and comparison with experimental data for the pedestal density models are shown in Section 4. In Section 5, conclusions are presented.

2. H-Mode Pedestal Temperature Model

In the development of the pedestal temperature models described in Onjun *et al.* (Onjun 2002), two ingredients are required: the pedestal width (Δ) and the pressure gradient ($\partial p/\partial r$). The pedestal density, n_{ped}, is obtained directly from the experiment or from the pedestal density model described in Section 4. The temperature at the top of the pedestal (T_{ped}) can be estimated as

$$T_{ped} = \frac{1}{2 n_{ped} k} \left| \frac{\partial p}{\partial r} \right| \Delta \qquad (1)$$

where k is the Boltzmann constant. Six pedestal models were developed based on Eq. (1) in the work by T. Onjun *et al.* (Onjun 2002). These pedestal temperature models are based on (1) the magnetic and flow shear stabilization width model [$\Delta \propto \rho s^{2}$] (Sugihara *et al.*, 2000), (2) the flow shear stabilization width model [$\Delta \propto (\rho R q)^{1/2}$] (Onjun *et al.*, 2002), (3) the normalized poloidal pressure width model [$\Delta \propto R(\beta_{\theta,ped})^{1/2}$] (Osborne *et al.*, 1999), (4) the diamagnetic stabilization width model [$\Delta \propto \rho^{2/3} R^{1/3}$] (Rogers *et al.*, 1999), (5) the ion orbit loss width model [$\Delta \propto \varepsilon^{1/2} \rho_\theta$] (Shaing 1992), and (6) the two fluid Hall equilibrium width model [$\Delta \propto (1/Z)(A_H/n_{ped})^{1/2}$] (Guzdar *et al.*, 2005). Note that the constant of proportionality in the pedestal width scaling based the two fluid Hall equilibrium width model in the work by P N Guzdar and his co-workers (Guzdar *et al.*, 2005) is varied in this work to improve agreement with experimental data. These six pedestal width models are used in this paper together with an improved pressure gradient model to develop new pedestal temperature models.

For the maximum pressure gradient in the pedestal of type I ELMy H-mode discharges, the pedestal pressure gradient is approximated as the pressure gradient limit of high-n ballooning modes in the short toroidal wavelength limit. The ballooning mode is usually described using the magnetic shear vs. normalized pressure gradient diagram (s-α diagram). Normally, the calculation of ballooning mode stability is complicated, requiring information about the plasma equilibrium and geometry. A number of different codes have been developed for stability analysis, such as HELENA, MISHKA and ELITE. In the work by T Onjun and his co-workers (Onjun *et al.*, 2004), stability analyses for JET triangularity scan H-mode discharges were carried out using the HELENA and MISHKA ideal MHD stability codes. For the JET high triangularity discharge 53298, the stability analysis results are shown in fig. 10 (Onjun *et al.*, 2004). Based on that result, the s-α MHD stability diagram with both the first and second stability effects included can be simplified as Fig. 1 in this paper. This s-α MHD stability diagram leads to an analytic expression for the critical normalized pressure gradient α_c that includes the effect of both the first and second stability of ballooning modes and geometrical effects given by:

$$\alpha_c \equiv -\frac{2\mu_0 R q^2}{B_T^2}\left(\frac{dp}{dr}\right)_c = \alpha_0(s)\left[\frac{1+\kappa_{95}^2\left(1+10\delta_{95}^2\right)}{7}\right]. \qquad (2)$$

where μ_0 is the permeability of free space, R is the major radius, q is the safety factor, B_T is the toroidal magnetic field, s is the magnetic shear, κ_{95} and δ_{95} are the elongation and triangularity at the 95% flux surface, and $\alpha_0(s)$ is a function of magnetic shear as

$$\alpha_0(s)=\begin{cases} 3+0.8(s-3) & s>6 \\ 6-3\sqrt{1-\left(\dfrac{6-s}{3}\right)^2} & 6\geq s\geq 3\,. \\ 6 & 3>s \end{cases} \qquad (3)$$

Note that the form of s-α MHD stability diagram in this work, the effect of geometry on the plasma edge stability has a similar form with that used in the work T. Onjun and his co-workers. (Onjun *et al.*, 2002), but somewhat stronger. The function in Eq. (3) can be understood as the following: for $s > 6$, the equation indicates that the pedestal is in the first stability regime of ballooning modes; for $6 \geq s \geq 3$, the equation represents the regime of a transition from first to second stability of ballooning modes; for $s < 3$, the equation represents a plasma that is in the second stability of ballooning modes, where the pedestal pressure gradient is limited by finite n ballooning mode stability. It should be noted that the effect of the current-driven peeling mode is not considered in this work. In Eq. (3), the bootstrap current and separatrix effects are included through the calculation of magnetic shear as described in in the work T. Onjun and his co-workers. (Onjun *et al.*, 2002). Note that the magnetic shear is calculated as

$$s = s_0\left(1-\frac{c_{bs}b(\upsilon^*,\varepsilon)\alpha_c}{4\sqrt{\varepsilon}}\right), \qquad (4)$$

where the multiplier C_{bs} is adjusted to account for the uncertainty of the bootstrap current effect.

3. Results and Discussions

Statistical comparisons between predicted pedestal parameters and corresponding experimental values obtained from the ITPA Pedestal Database (Hatae *et al.*, 2001) version 3.2 are carried out. To quantify the comparison between the predictions of each model and experimental data, the root mean-square error (RMSE), the offset, and the Pearson product moment correlation coefficient (R) are computed.

Six scalings for the pedestal temperature are derived using the six models described above for the width of the pedestal together with the model given by Eqs. (2) and (3) for the critical pressure gradient that includes both the first and second stability of ballooning modes. The pedestal temperature scalings are calibrated using 457 experimental data points (90 from JET experiment, and 367 from JT-60U experiment) for the ion pedestal temperature from the ITPA Pedestal Database (Version 3.2). The statistical results are shown in Table 1. The value of the coefficient, C_w, used in each of the expressions for the pedestal width and the value of multiplier C_{bs} used in the calculation of magnetic shear are given in the second and third column of Table 1, respectively. It is found that the RMSEs for the pedestal temperature range from 28.2% to 109.4%, where the model based on $\Delta \propto \rho s^2$ yields the lowest RMSE. For the offset, it is shown in Table 1 that the offsets range from -6.5% to 9.0%, where the model based on $\Delta \propto \rho s^2$ yields the best agreement (smallest absolute value of the offset). For the correlation R, it is shown in Table 1 that the values of correlation R range from 0.28 to 0.80, where the model based on $\Delta \propto \rho s^2$ yields the best agreement (highest value of R). From these results, it can be concluded that the pedestal temperature based on $\Delta \propto \rho s^2$ yields the best average agreement with experimental data. The comparisons between the predictions of the models based on $\Delta \propto \rho s^2$ and experimental data are shown in Figs. 2. It can be seen that the predictions of pedestal temperature are in reasonable agreement with experimental data.

4. H-Mode Pedestal Density Model

In the development of the pedestal density model, an empirical approach is employed. In the work by J Hughes *et al.* (Hughes *et al.*, 2002), a pedestal density scaling is developed for Alcator CMOD H-mode discharges. This scaling is expressed as a function of the line average density, plasma current (I_p), and toroidal magnetic field (B_T). Using this kind of power law regression fit for the 626 data points in the ITPA Pedestal Database (Version 3.2), the best predictive pedestal density scaling for type I ELMy H-mode discharges is found to be

$$n_{ped}\left[10^{20}\mathrm{m}^{-3}\right] = 0.74\left(n_l\left[10^{20}\mathrm{m}^{-3}\right]\right)^{0.99}\left(I_p\left[MA\right]\right)^{0.15}\left(B_T\left[T\right]\right)^{-0.12}. \quad (5)$$

This scaling yields an RMSE of 10.9%, R^2 of 0.97, and offset of 3.3% with a data set of 626 data points (132 from ASDEX-U experiment, 127 from JET experiment, and 367 from JT-60U experiment). The comparisons of the density models' predictions for the pedestal density using Eq. (5) and the experimental data are shown in Fig. 3. In the figure, the agreement is good for a low ratio of pedestal density to the Greenwald density. However, the agreement tends to break away at high density. This might indicate that the physics that controls low and high edge density might be different.

5. Pedestal Prediction in ITER

The pedestal temperature and density models developed in this paper are used to predict the pedestal parameters for the ITER design. For an ITER standard H-mode discharge with 15 MA plasma current and the line average density of $1.05\mathrm{x}10^{20}$ particles/m^3, the pedestal density is predicted to be 0.95 $\mathrm{x}10^{20}$ particles/m^3. It is worth noting that the pedestal density using Eq.(5) indicate a flat density profile since the pedestal density is almost the same as the line average density. This observation is often observed in H-mode experiments with high density. In addition, the pedestal density in ITER predicted using an integrated modeling code JETTO yields similar result for the density profile (Onjun *et al.*, 2005). The pedestal temperature model based on the width of the pedestal as $\Delta \propto \rho s^2$ and the critical pressure gradient model that includes both first and second stability of ballooning modes is used to predict the pedestal temperature in ITER. Figure 4 shows the predicted pedestal temperature as a function of pedestal density. It can be seen that the pedestal temperature decreases as the pedestal density increases. At the predicted pedestal density, the predicted pedestal temperature is 1.7 keV. Under these conditions, it is found that the pedestal width in ITER predicted by the model ranges about 4 cm.

6. Conclusions

Pedestal temperature models that include the effects of both the first and second stability of ballooning modes are developed for type I ELMy H-mode plasmas in tokamaks. The results for the pedestal temperature are compared with experimental data obtained from the ITPA Pedestal Database version 3.2. It is found that the pedestal temperature model based on the magnetic and flow shear stabilization yields the best agreement with experimental data (with RMSE of 28.2%). It is found that the prediction of pedestal temperatures for ITER using the pedestal temperature and density models developed is 1.7 keV.

7. Acknowleagement

I am grateful to Prof. Suthat Yoksan, Prof. Arnold H. Kritz, Dr. Glenn Bateman, Dr.Vassili Parail and Dr. Alexei Pankin for their helpful discussions and supports. Also, I thank the ITPA Pedestal Database group for the pedestal data used in this work. This work is supported by Commission on Higher Education and the Thailand Research Fund (TRF) under Contract No. MRG4880165.

8. Referecnes

Aymar, R., Barabaschi, P. & Shimomura, Y. (for the ITER team) (2002). The ITER design. *Plasma Phys. Control. Fusion* **44**, 519.

Deutsch, C. (2004). Penetration of intense charged particle beams in the outer layers of precompressed thermonuclear fuels. *Laser Part. Beams* **22** (2), 115-120.

Deutsch, C., Bret, A. & Fromy, P. (2005). Mitigation of electromagnetic instabilities in fast ignition scenario. *Laser Part. Beams* **23** (1), 5-8.

Greenwald, M., Boivin, R.L., Bombarda, F., *et al.* (1997), H-mode confinement in Alcator C-Mod. *Nuclear Fusion* **37**, 793.

Guzdar, P N, Mahajan, S.M., & Yoshida, Z. (2005) A theory for the pressure pedestal in high (H) mode tokamak discharges *Physics of Plasmas* **12** 032502.

Hatae, T., Sugihara, M., Hubbard, A.E. *et al.*, (2001) Understanding of H mode pedestal characteristics using the multimachine pedestal database *Nucl. Fusion* **41** 285.

Hora, H. (2004). Developments in inertial fusion energy and beam fusion at magnetic confinement. *Laser Part. Beams* **22** (4), 439-449.

Hughes, J. W.,Mossessian, D.A., Hubbard, A.E. *et al.*, (2002) Observations and empirical scalings of the high-confinement mode pedestal on Alcator C-Mod *Physics of Plasmas* **9** 3019.

Kinsey J.E., Bateman G., Onjun T., *et al.* (2003) Burning plasma projections using drift-wave transport models and scalings for the H-mode pedestal *Nucl. Fusion* **43** 1845

Li, X.Z., Liu, B., Chen, S., Wei, Q.M. & Hora, H. (2004). Fusion cross-sections for inertial fusion energy. *Laser Part. Beams* **22** (4), 469-477.

Mulser, P. & Bauer, D. (2004). Fast ignition of fusion pellets with superintense lasers: Concepts, problems, and prospectives. *Laser Part. Beams* **22** (1), 5-12.

Onjun, T., Bateman, G., Kritz, A.H. & Hammett G. (2002), Models for the pedestal temperature at the edge of H-mode tokamak plasmas. *Physics of Plasmas* **9**, 5018.

Onjun T., Kritz A.H., Bateman, G. *et al.*, (2004) Integrated pedestal and core modeling of Joint European Torus (JET) triangularity scan discharges *Phys. Plasmas* **11** 3006.

Onjun, T., Kritz A.H., Bateman, G. *et al.*, (2005) Magnetohydrodynamic-calibrated edge-localized mode model in simulations of International Thermonuclear Experimental Reactor *Physics of Plasmas* **12** 082513.

Onjun (2006) Pedestal temperature models based on first and second stability limits of ballooning modes *Laser and Particle Beams* 24, 113-116.

Osborne, T.H., Burrell, K.H., Groebner, R.J., *et al.* (1999), H-mode pedestal characteristics in ITER shape discharges on DIII-D. *Journal of Nuclear Materials* **266-269**, 131.

Rogers, B.N. & Drake, J.F.(1999) Diamagnetic stabilization of ideal ballooning modes in the edge pedestal. *Phys. Plasmas* **6** 2797.

Shaing, K.C. (1992) Poloidal magnetic field dependence of the edge electric field layer width in the H mode in tokamaks *Phys. Fluids B* **4** 290.

Sugihara, M., Igitkhanov, Yu., Janeschitz, G., *et al.* (2000), A model for H-mode pedestal width scaling using the International Pedestal Database. *Nuclear Fusion* **40**, 1743.

Table 1: Statistical results of the models for type 1 ELMy H-mode discharges.

Pedestal width scaling	C_w	C_{bs}	RMSE (%)	Offset (%)	R
$\Delta \propto \rho s^2$	5.10	3.0	28.2	0.5	0.80
$\Delta \propto (\rho R q)^{1/2}$	0.22	4.5	35.4	2.9	0.75
$\Delta \propto R(\beta_{\theta,\mathrm{ped}})^{1/2}$	1.50	3.7	35.5	-1.0	0.73
$\Delta \propto \rho^{2/3} R^{1/3}$	1.37	4.9	49.3	-1.1	0.67
$\Delta \propto \varepsilon^{1/2} \rho_\theta$	2.75	4.9	109.4	9.0	0.28
$\Delta \propto (1/Z)(A_H/n_{\mathrm{ped}})^{1/2}$	0.014	5.9	50.5	-6.5	0.68

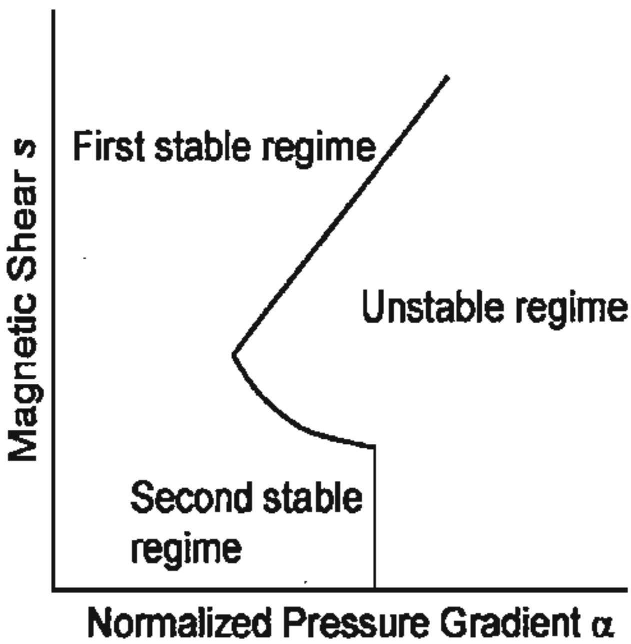

Fig. 1: The normalized pressure gradient vs. magnetic shear diagram (s-α diagram) is plotted. First and second stability region and unstable region is also described.

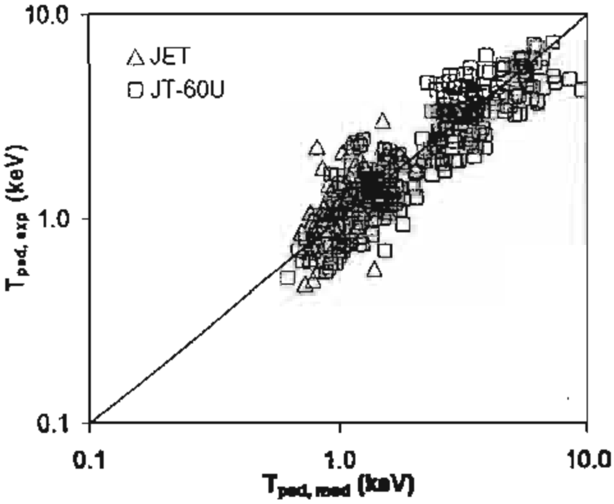

Fig. 2: Experimental ion pedestal temperature for type I H-mode plasmas compared with the model predictions based on $\Delta \propto \rho s^2$.

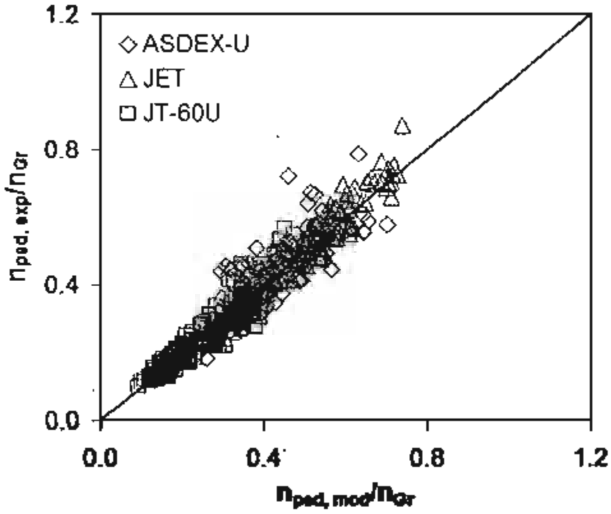

Fig. 3: The ratios of experimental pedestal electron density for type I H-mode plasmas to the Greenwald density are compared with the ratio of the model predictions using Eq. (6) to the Greenwald density.

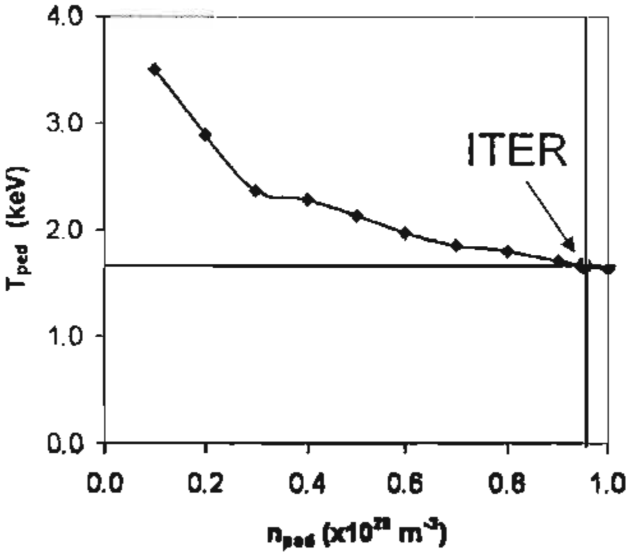

Fig. 4: Predictions of pedestal temperature as a function of pedestal density using the pedestal temperature model based on $\Delta \propto \rho s^2$

Self-consistent modeling of ITER with BALDUR integrated predictive modeling code

Thawatchai Onjun
Sirindhorn International Institute of Technology, Thammasat University,
Klong Luang, Pathumthani, 12121, Thailand
E-mail: thawatchai@siit.tu.ac.th

Abstract

Self-consistent modeling of the International Thermonuclear Experimental Reactor (ITER) has been carried out using the BALDUR integrated predictive modeling code together with either the Mixed Bohm/gyro-Bohm (Mixed B/gB) core transport model or Multimode (MMM95) core transport model. The pedestal values are obtained from the theoretical-based model using a neoclassical transport in the JETTO integrated predictive modeling code. It is found that simulations of ITER with a standard H-mode scenario yield fusion Q in the range of 0.9 to 12.5, which depends on the core transport model and the value of pedestal temperature. The simulations using MMM95 core transport tends to be more optimistic than those using Mixed B/gB. To reach fusion Q of 10, the BALDUR simulation with Mixed B/gB requires the pedestal temperature higher than that used in the BALDUR simulation with MMM95 core transport model.

Keywords: Plasma; H-mode; ELMs; Pedestal; Simulation; ITER

1. Introduction

The International Thermonuclear Experimental Reactor (ITER) is an international collaborative effort with the aim to demonstrate the scientific and technological feasibility of fusion energy (Aymar *et al.*, 2002) using magnetic confinement fusion concept. While in inertial fusion, another possible approach for fusion research, the discussion for the most appropriate way to ignite a fusion pellet is still going on and is concerned with instabilities (Deutsch *et al.*, 2005), and the interaction of charge particle and laser beams with dense plasma (Deutsch 2004; Mulser *et al.*, 2004), the underlying nuclear physics is similar for both approaches (Hora 2004; Li *et al.*, 2004), the step with ITER is an important step for magnetic confinement fusion research. With a decision to construct the device in France, this big step forward has been taken to explore the properties of long burning plasma. In this paper, the performance of ITER based on its standard H-mode scenario is investigated using an integrated predictive integrated modeling code BALDUR with two different core transport models. It is important to simulate plasma behaviors in ITER and to predict the ITER performance, which will lead to a way to optimize or to improve the performance in order to have a better chance of success.

Achieving fusion ignition is one of the goals in fusion study of ITER. Due to the fact that H-mode discharges in tokamaks generally provide excellent energy confinement and have acceptable particle transport rates for impurity control, burning plasma experiments, such as ITER, are designed to operate in the high mode (H-mode) regime. According to previous ITER study by G. Bateman and his co-workers (Bateman *et al.*, 2003), a BALDUR integrated predictive modeling code with a Multi-mode (MMM95) core transport model was used to predict the plasma core profiles of ITER and, consequently, the ITER performance. The boundary conditions, which were taken to be at the top of the pedestal, were obtained from a predictive pedestal model based on magnetic and flow shear stabilization width model and first stability regime of ballooning modes (Onjun *et al.*, 2002). The performance of ITER was expressed in term of fusion Q. Note that fusion Q is the ratio of a fusion power with an applied heating power. According to the ITER simulations carried out using BALDUR code, an optimistic performance of ITER was obtained with fusion Q of 10.6. In the later ITER study by T. Onjun and his co-workers (Onjun *et al.*, 2005), ITER simulations were carried out using a JETTO integrated predictive modeling code with a Mixed Bogm/gyro-Bohm (Mixed B/gB) core transport model, which predicted a more optimistic performance with fusion Q of 16.6. It was also found that the JETTO code predicts the strong edge pressure gradient, which is in the second stability regime of ballooning modes. In other words, the values at top of the pedestal in JETTO simulation are higher than those used in BALDUR code.

In this work, a BALDUR integrated predictive modeling code is used to simulate the core profiles in ITER standard H-mode scenario by using two different core transport models (MMM95 or Mixed B/gB) together with the pedestal values obtained from the JETTO simulations in the work by T. Onjun and his co-workers (Onjun *et al.*, 2005). The paper is organized as follow: A brief descriptions for a BALDUR integrated predictive modeling code and both core transport models are addressed in Sec.2. The ITER prediction using a BALDUR integrated predictive modeling code is described in Sec. 3, while conclusions are given in Sec. 4.

2. BALDUR integrated predictive modeling code

The BALDUR integrated predictive modeling code (Singer *et al*., 1988) is used to compute the time evolution of plasma profiles including electron and ion temperature, deuterium and tritium density, helium and impurity density, magnetic q, neutrals, and fast ions. These time-evolving profiles are computed in the BALDUR integrated predictive modeling code by combining the effects of many physical processes self-consistently, including the effects of transport, plasma heating, particle influx, boundary conditions, the plasma equilibrium shape, and sawtooth oscillations. Fusion heating and helium ash accumulation are computed self-consistently. The BALDUR simulations have been intensively compared against various plasma experiments, which yield an over all agreement of 10% RMS deviation (Onjun *et al*. (2001); Hannum *et al*. (2001)). In this work, two core transport models in BALDUR will be used to carry out simulations of ITER. The brief details of these transport models are described below.

2.1 Mixed B/gB core transport model

The Mixed B/gB core transport model (Erba *et al*. (1997)) is an empirical transport model. It was originally a local transport model with Bohm scaling. A transport model is said to be "local" when the transport fluxes (such as heat and particle fluxes) depend entirely on local plasma properties (such as temperatures, densities, and their gradients). A transport model is said to have "Bohm" scaling when the transport diffusivities are proportional to the gyro-radius times thermal velocity over a plasma linear dimension such as major radius. Transport diffusivities in models with Bohm scaling are also functions of the profile shapes (characterized by normalized gradients) and other plasma parameters such and magnetic q, which are all assumed to be held fixed in systematic scans in which only the gyro-radius is changed relative to plasma dimensions.

The original JET model was subsequently extended to describe ion transport, and a gyro-Bohm term was added in order for simulations to be able to match data from smaller tokamaks as well as data from larger machines. A transport model is said to have "gyro-Bohm" scaling when the transport diffusivities are proportional to the square of the gyroradius times thermal velocity over the square of the plasma linear dimension. The Bohm contribution to the JET model usually dominates over most of the radial extent of the plasma. The gyro-Bohm contribution usually makes its largest contribution in the deep core of the plasma and plays a significant role only in smaller tokamaks with relatively low power and low magnetic field.

2.2 Multimode core transport model

The MMM95 model (Bateman *et al*. (1998)) is a linear combination of theory-based transport models which consists of the Weiland model for the ion temperature gradient (ITG) and trapped electron modes (TEM), the Guzdar–Drake model for drift-resistive ballooning modes, as well as a smaller contribution from kinetic ballooning modes. The Weiland model for drift modes such as ITG and TEM modes usually provides the largest contribution to the MMM95 transport model in most of the plasma core. The Weiland model is derived by linearizing the fluid equations, with magnetic drifts for each plasma species. Eigenvalues and eigenvectors computed from these fluid equations are then used to compute a quasilinear approximation for the thermal and particle transport fluxes. The Weiland model includes many different physical phenomena such as effects of trapped electrons, $T_i \neq T_e$, impurities, fast ions, and finite b. The resistive ballooning model in MMM95 transport model is based on the 1993 ExB drift-resistive ballooning mode model by Guzdar–Drake, in which the transport is proportional to the pressure gradient and collisionality. The contribution from the resistive ballooning model usually dominates the transport near the plasma edge. Finally, the kinetic ballooning model is a semi-empirical model, which usually provides a small contribution to the total diffusivity throughout the plasma, except near the magnetic axis. This model is an approximation to the first ballooning mode stability limit. All the anomalous transport contributions to the MMM95 transport model are multiplied by κ^{-4}, since the models were originally derived for circular plasmas.

3. ITER simulations using BALDUR code

The ITER simulation is carried out using the BALDUR integrated predictive modeling code with the designed parameters shown in Table 1. The core transport is calculated using either the Mixed B/gB core transport model or the MMM95 core transport model. The boundary conditions are the values at the top of the pedestal, which are obtained from the work by T. Onjun and coworkers (Onjun *et al.*, 2005), where an anomalous transport is fully suppressed and neoclassical transport is fully governs the pedestal region. In addition, an instability driven either by an edge pressure gradient or by an edge current can trigger ELM crashes, which limits the height of the pedestal. The predictions of electron and ion pedestal temperature are summarized in Fig. 1. It can be seen that ion temperature is higher than electron temperature and the pedestal temperatures increase as the pedestal increases. The auxiliary heating power used in these simulations is the combination of 33 MW NBI heating with 7 MW of RF heating.

Simulations of ITER are carried out using either the Mixed B/gB core transport model or the MMM95 core transport model in the BALDUR code in which the value of the pedestal width is varied from 2 to 8 cm (the pedestal temperature is varied following Fig.1). It can be seen in Figs. 2 and 3 that the ion and electron temperature profiles tend to be peak. For the density profiles, the simulations with Mixed B/gB core transport model tend to be flat at low pedestal width (low pedestal temperature), but tend to be peak at high pedestal width (high pedestal temperature). On the other hands, the simulations with MMM95 core transport model tend to be flat for all values of the pedestal width. The relatively flat profiles are also obtained in the previous ITER studies (Bateman *et al.*, 2003; Onjun *et al.*, 2005). In Fig. 4, it shows the increase of central ion temperature (top panel) and central electron temperature (bottom panel) as a function of pedestal width (in turn, the pedestal temperature). It can be seen that the central temperatures for both ion and electron obtained using BALDUR code with either Mixed B/gB or MMM95 are in the range between 10 keV to 20 keV; while the JETTO simulations using Mixed B/gB (Onjun *et al.*, 2005) produce higher central temperature, even though the same pedestal values are used. Note that the purpose of this paper is to show the performance of ITER designed. The difference in the predictions of BALDUR and JETTO code with Mixed B/gB needs a further analysis. We rather leave this issue for future work.

In Fig. 5, fusion Q at the time of 300 sec is plotted as a function of the pedestal width. It can be seen that fusion Q increases as the pedestal width increases. This increase can be explained by the increase of pedestal temperatures, which leads to an increase of central temperatures. Based on the ITER design, the performance of ITER is expected to reach fusion Q of 10. Based on Fig. 5, to reach fusion Q of 10, the BALDUR simulations with Mixed B/gB require the pedestal width greater than 8 cm, which means the pedestal temperature higher than 6 keV. However, the BALDUR simulations with MMM95 core transport model require the pedestal width about 6 cm (3% of the minor radius), which means the pedestal temperature between 4 to 5 keV. Note that the pedestal width of H-mode plasma typically extends over with a width of less than 5% of the plasma minor radius.

4. Conclusions

Self-consistent simulations of ITER have been carried out using the BALDUR integrated predictive modeling. Simulations are carried out either using MMM95 core transport model or using Mixed B/gB core transport model with the pedestal values obtained from the model based on the neoclassical transport in JETTO code. It is found that the standard H-mode scenario simulation of the ITER design yields fusion Q in the range of 1.0 to 13.3, which depends on the core transport model and the value of pedestal width used. The simulations using MMM95 core transport tends to be more optimistic than those using Mixed B/gB. To reach fusion Q of 10, the BALDUR simulations with Mixed B/gB requires the pedestal width greater than 8 cm (means the pedestal temperature higher than 6 keV); while the BALDUR simulations with MMM95 core transport model requires the pedestal width about 6 cm (means the pedestal temperature between 4 to 5 keV).

5. Acknowleagement

I am grateful to Prof. Suthat Yoksan, Prof. Arnold H. Kritz, Dr. Glenn Bateman, Dr.Vassili Parail and Dr. Alexei Pankin for their helpful discussions and supports. Also, I thank the ITPA Pedestal Database group for the pedestal data used in this work. This work is supported by Commission on Higher Education and the Thailand Research Fund (TRF) under Contract No. MRG4880165.

6. References

Aymar, R., Barabaschi, P. & Shimomura, Y. (for the ITER team) (2002). The ITER design. *Plasma Phys. Control. Fusion* **44**, 519.

Bateman, G., Kritz, A.H., Kinsey J. *et al.*, (1998) Predicting temperature and density profiles in tokamaks. *Physics of Plasmas* **5** 1793-1799.

Bateman, G., Onjun, T. & Kritz, A. H. (2003). Integrated predictive modelling simulations of burning plasma experiment designs *Plasma Phys. Control. Fusion* **45**, 1939-1960.

Deutsch, C. (2004). Penetration of intense charged particle beams in the outer layers of precompressed thermonuclear fuels. *Laser Part. Beams* **22** (2), 115-120.

Deutsch, C., Bret, A. & Fromy, P. (2005). Mitigation of electromagnetic instabilities in fast ignition scenario. *Laser Part. Beams* **23** (1), 5-8.

Erba, M., Cherubini, A., Parail, V.V. *et al.*, (1997) Development of a non-local model for tokamak heat transport in L-mode, H-mode and transient regimes. *Plasma Phys. Control. Fusion* **39**, 261-276.

Hannum, D., Bateman, G., Kinsey, J. *et al.*, (2001) Comparison of high-mode predictive simulations using Mixed Bohm/gyro-Bohm and Multi-Mode (MMM95) transport models. *Physics of Plasmas* **8** 975-985.

Hora, H. (2004). Developments in inertial fusion energy and beam fusion at magnetic confinement. *Laser Part. Beams* **22** (4), 439-449.

Li, X.Z., Liu, B., Chen, S., Wei, Q.M. & Hora, H. (2004). Fusion cross-sections for inertial fusion energy. Laser Part. Beams 22 (4), 469-477.

Mulser, P. & Bauer, D. (2004). Fast ignition of fusion pellets with superintense lasers: Concepts, problems, and prospectives. Laser Part. Beams 22 (1), 5-12.

Onjun, T., Bateman, G., Kritz A.H. et al., (2001) Comparison of low confinement mode transport simulations using the mixed Bohm/gyro-Bohm and the Multi-Mode-95 transport model. Physics of Plasmas 8 975-985.

Onjun, T., Bateman, G., Kritz, A.H. & Hammett G. (2002), Models for the pedestal temperature at the edge of H-mode tokamak plasmas. Physics of Plasmas 9, 5018.

Onjun, T., Kritz A.H., Bateman, G. et al., (2005) Magnetohydrodynamic-calibrated edge-localized mode model in simulations of International Thermonuclear Experimental Reactor. Physics of Plasmas 12 082513.

Singer, C.E., Post, D.E., Mikkelsen, D.R. et al., (1988) BALDUR: a one-dimensional plasma transport code. Comput. Phys. Commun. 49 399.

Table 1: The basic parameters for ITER design

Parameters	Values
Major radius	6.2 m
Minor radius	2.0 m
Plasma current	15 MA
Toroidal magnetic field	5.3 T
Elongation	1.70
Triangularity	0.33
Line average density	1.0×10^{20} m^{-3}
Effective charge	1.4
Auxiliary power	40 MW

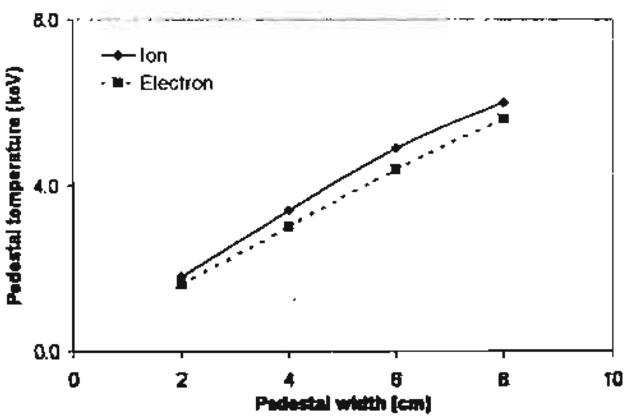

Fig. 1: The ion and electron temperatures at the top of the pedestal are plotted as a function of pedestal width. These results are obtained using a JETTO integrated predictive modeling code with Mixed B/gB core transport model.

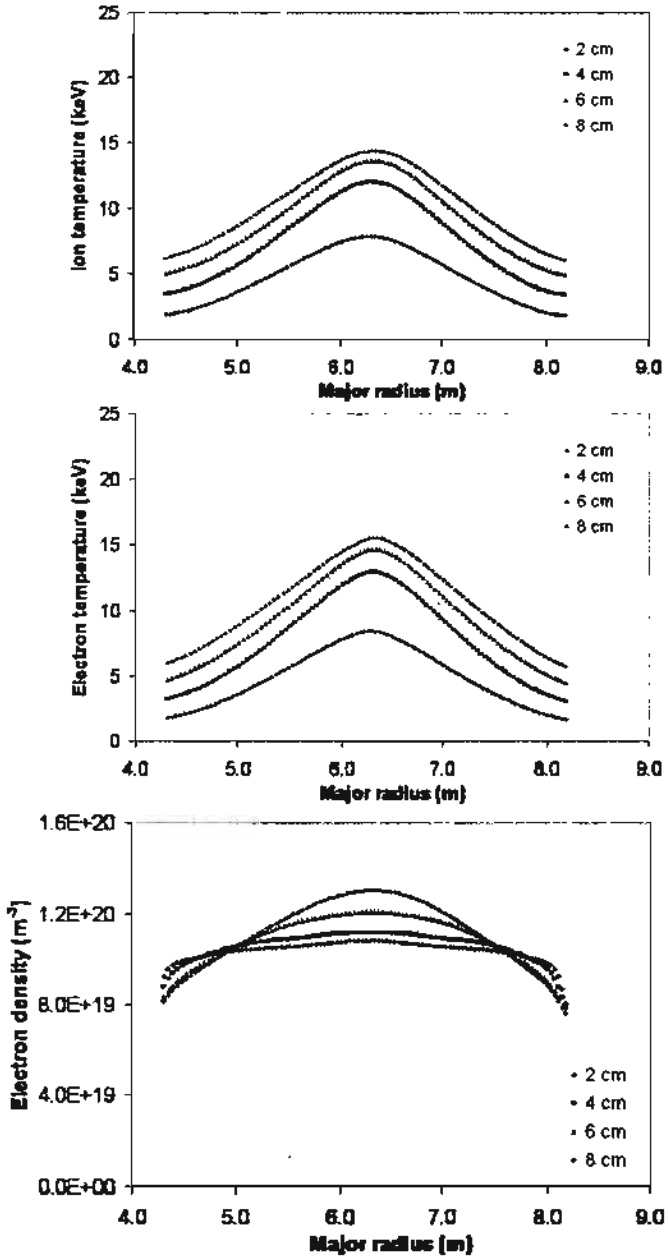

Fig. 2: Profiles for ion (top) and electron (middle) temperatures and electron density (bottom) are shown as a function of major radius at a time of 300 sec. These BALDUR simulations are carried out using Mixed B/gB core transport model for different values of pedestal temperature.

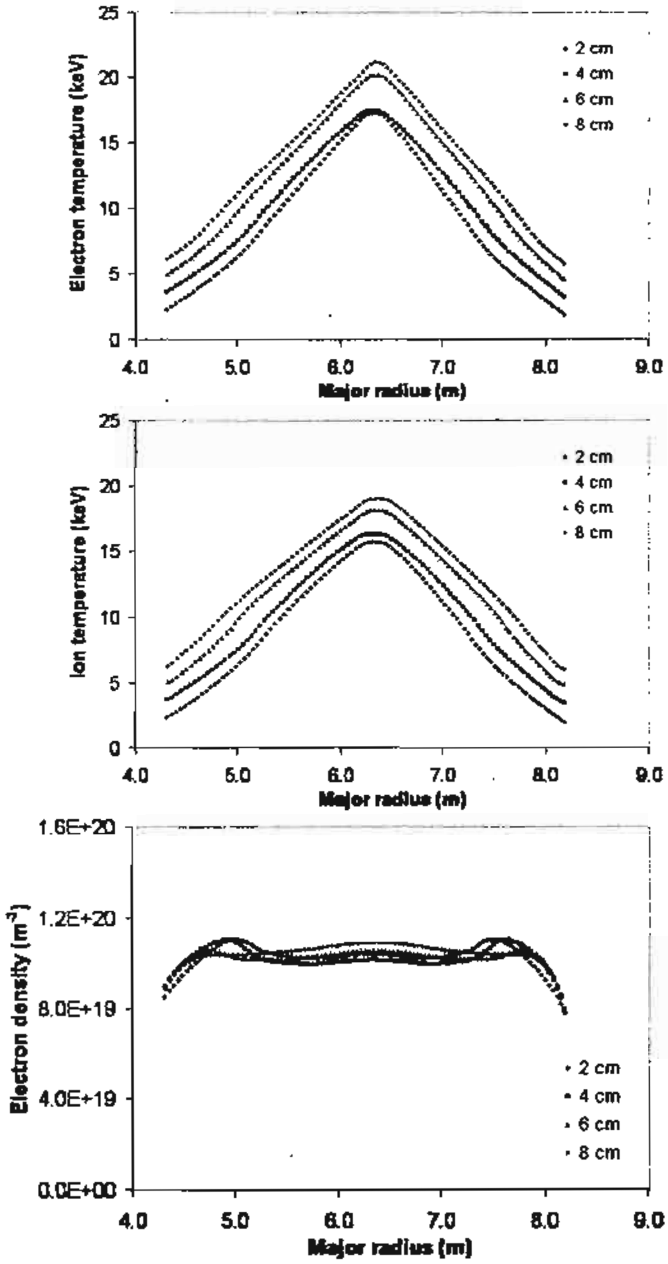

Fig. 3: Profiles for ion (top) and electron (middle) temperatures and electron density (bottom) are shown as a function of major radius at a time of 300 sec. These BALDUR simulations are carried out using MMM95 core transport model for different values of pedestal temperature.

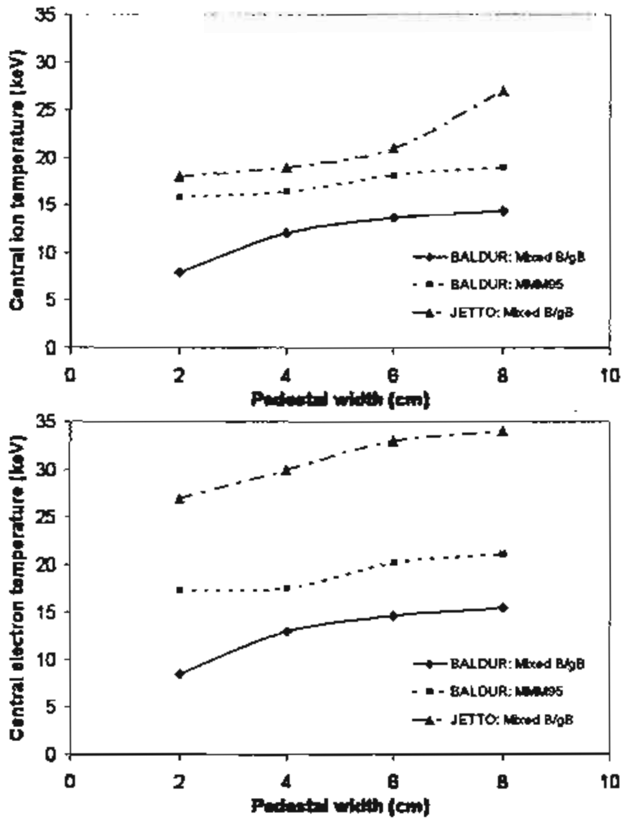

Fig. 4: The central ion (top) and electron (bottom) temperatures are plotted as a function of pedestal width. The solid line and dotted line are the results from the BALDUR predictions either using Mixed B/gB core transport code or using MMM95 core transport model, respectively; while the dot-dashed line is result from the JETTO predictions using Mixed B/gB core transport code.

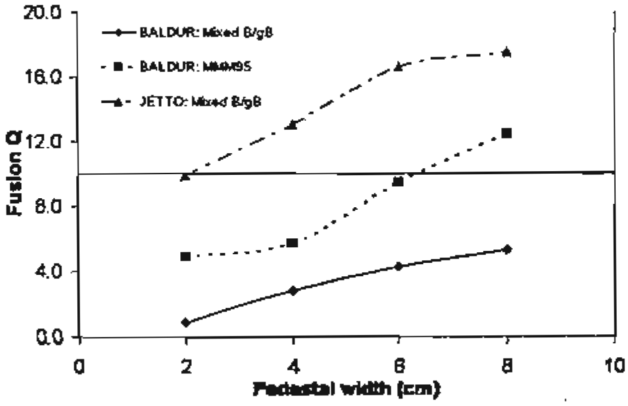

Fig. 5: Fusion Q is plotted as a function of pedestal width. The solid line and dotted line are the results from the BALDUR predictions either using Mixed B/gB core transport code or using MMM95 core transport model, respectively; while the dot-dashed line is result from the JETTO predictions using Mixed B/gB core transport code.

บทความทางวิชาการที่ตีพิมพ์เป็น Proceeding ในการประชุมวิชาการนานาชาติ The

21st IAEA Fusion Energy Conference:

T. Onjun, A.H. Kritz, G. Bateman, andA. Pankin "Second Ballooning Stability Effect on H-mode Pedestal Scalings" *in Proc. of the 21st IAEA Fusion Energy Conference* 16 - 21 October 2006, Chengdu, China,

ISBN 92-0-100907-0 / ISSN 0074-1884

Second Ballooning Stability Effect on H-mode Pedestal Scalings

T. Onjun 1), A.H. Kritz 2), G. Bateman 2), A. Pankin 2)

1) Sirindhorn International Institute of Technology, Klong Luang, Pathumthani, Thailand
2) Department of Physics, Lehigh University, Pennsylvania, USA

E-mail: thawatchai@siit.tu.ac.th

Abstract. Models for the prediction of ion and electron pedestal temperatures at the edge of type I ELMy H-mode plasmas are developed. These models are based on theory motivated concepts for pedestal width and pressure gradient. The pedestal pressure gradient is assumed to be limited by high *n* ballooning mode instabilities, where both the first and second stability limits are considered. The effect of the bootstrap current, which reduces the magnetic shear in the steep pressure gradient region at the edge of the H-mode plasma, can result in access to the second stability of ballooning mode. In these pedestal models, the magnetic shear and safety factor are calculated at a radius that is one pedestal width away from separatrix. The predictions of these models are compared with pedestal data for type I ELMy H-mode discharges obtained from the latest public version (version 3.2) in the International Tokamak Physics Activity Edge (ITPA) Pedestal Database. It is found that the pedestal temperature model based on the magnetic and flow shear stabilization yields the best agreement with experimental data (RMSE of 28.2%). For standard H-mode ITER discharges with 15 MA plasma current, predictive analysis yields ion and electron temperatures at the top of the H-mode pedestal in the range from 1.7 to 1.9 keV.

1. Introduction

It is well known that when the plasma heating power increases, plasmas can undergo a spontaneous self-organizing transition from a low confinement mode (L-mode) to a high confinement mode (H-mode). This plasma activity is widely believed to be caused by the generation of a flow shear at the edge of plasma, which is responsible for suppressed turbulence and transport near the edge of plasma. The reduction of transport near the plasma edge results in a narrow sharply-defined region at the edge of the plasma with steep temperature and density gradients, called the pedestal. This pedestal is located near the last closed magnetic flux surface and typically extends over with a width of about 5% of the plasma minor radius. It was found that energy confinement in the H-mode regime of tokamaks strongly depends on the temperature and density at the top of the pedestal [1]. Therefore, it is important in H-mode tokamak plasma studies, especially for the burning plasma experiment such as the International Thermonuclear Experimental Reactor (ITER) [2], to have a reliable prediction for temperatures at the top of the pedestal.

In the previous pedestal study by T. Onjun *et al.* [3], six theory-based pedestal temperature models were developed using different models for the pedestal width together with a ballooning mode pressure gradient limit that is restricted to the first stability of ballooning modes. These models also include the effects of geometry, bootstrap current, and separatrix, leading to a complicated nonlinear behavior. For the best model, the agreement between model's predictions and experimental data for pedestal temperature is about 30.8% RMSE for 533 data points from the International Tokamak Physics Activity Edge (ITPA) Pedestal Database. One weakness of these pedestal temperature models is the assumption that the plasma pedestal is in the first stability regime of ballooning modes.

In this study, six pedestal width models in Refs. [3-8] are modified to include the effect of the second stability limit of ballooning modes. The predictions from these pedestal temperature models are be tested against the latest public version of the pedestal data (Version 3.2) obtained from the ITPA Pedestal Database. This paper is organized in the following way: In Section 2, the pedestal temperature model development is described. In Section 3, the predictions of the pedestal temperature resulting from the models are compared with pedestal temperature experimental data. A simple statistical analysis is used to characterize the agreement of the predictions of each model with experimental data. The development and comparison with experimental data for the pedestal density models are shown in Section 4. In Section 5, conclusions are presented

2. H-Mode Pedestal Temperature Model

Each pedestal temperature model described in Ref. [1] has two parts: a model for the pedestal width (Δ) and a model for the pressure gradient ($\partial p/\partial r$). The pedestal density, n_{ped}, is obtained directly from the experiment or from the pedestal density model described in Section 4. The temperature at the top of the pedestal (T_{ped}) can be estimated as

$$T_{ped} = \frac{1}{2 n_{ped} k} \left| \frac{\partial p}{\partial r} \right| \Delta \qquad (1)$$

where k is the Boltzmann constant. Six pedestal models were developed based on Eq. (1) in Ref. [3]. These pedestal models are based on (1) the flow shear stabilization width model [$\Delta \propto (\rho R q)^{1/2}$] [3], (2) the magnetic and flow shear stabilization width model [$\Delta \propto \rho s^2$] [4], (3) the normalized poloidal pressure width model [$\Delta \propto R(\beta_{\theta,ped})^{1/2}$] [5], (4) the diamagnetic stabilization width model [$\Delta \propto \rho^{2/3} R^{1/3}$] [6], (5) the ion orbit loss width model [$\Delta \propto \varepsilon^{1/2} \rho_\theta$] [7], and (6) the two fluid Hall equilibrium width model [$\Delta \propto (1/Z)(A_H/n_{ped})^{1/2}$] [8]. Note that the constant of proportionality in the pedestal width scaling based the two fluid Hall equilibrium width model in Ref. [8] is varied in this work to improve agreement with experimental data. These six pedestal width models are used in this paper together with an improved pressure gradient model to develop new pedestal temperature models.

For the maximum pressure gradient in the pedestal of type I ELMy H-mode discharges, the pedestal pressure gradient is approximated as the pressure gradient limit of high-n ballooning modes in the short toroidal wavelength limit. The ballooning mode is usually described using the magnetic shear vs. normalized pressure gradient diagram (s-α diagram). Normally, the calculation of ballooning mode stability is complicated, requiring information about the plasma equilibrium and geometry. A number of different codes have been developed for stability analysis, such as HELENA, MISHKA and ELITE. In Ref. [9], stability analyses for JET triangularity scan H-mode discharges were carried out using the HELENA and MISHKA ideal MHD stability codes. For the JET high triangularity discharge 53298, the stability analysis results are shown in fig. 10 in Ref. [9]. Based on results obtained in Ref. [9], the s-α MHD stability diagram with both the first and second stability effects included can be simplified as Fig. 1. This s-α MHD stability diagram leads to an analytic expression for the critical normalized pressure gradient α_c that includes the effect of both the first and second stability of ballooning modes and geometrical effects given by:

$$\alpha_c \equiv -\frac{2\mu_0 R q^2}{B_T^2}\left(\frac{dp}{dr}\right)_c = \alpha_0(s)\left[\frac{1+\kappa_{95}^2\left(1+10\delta_{95}^2\right)}{7}\right]. \quad (2)$$

where μ_0 is the permeability of free space, R is the major radius, q is the safety factor, B_T is the toroidal magnetic field, s is the magnetic shear, κ_{95} and δ_{95} are the elongation and triangularity at the 95% flux surface, and $\alpha_0(s)$ is a function of magnetic shear as

$$\alpha_0(s) = \begin{cases} 3+0.8(s-4) & s>6 \\ 6-3\sqrt{1-\left(\dfrac{6-s}{3}\right)^2} & 6\geq s\geq 3. \\ 6 & 3>s \end{cases} \quad (3)$$

Note that in this work, the effect of geometry on the plasma edge stability has a similar form with that used in Ref. [3], but somewhat stronger. The function in Eq. (3) can be understood as the following: for $s > 6$, the equation indicates that the pedestal is in the first stability regime of ballooning modes; for $6 \geq s \geq 3$, the equation represents the regime of a transition from first to second stability of ballooning modes; for $s < 3$, the equation represents a plasma that is in the second stability of ballooning modes, where the pedestal pressure gradient is limited by finite n ballooning mode stability. It should be noted that the effect of the current-driven peeling mode is not considered in this work. In Eq. (3), the bootstrap current and separatrix effects are included through the calculation of magnetic shear as described in Ref. [1]. Note that the magnetic shear in Ref. [3] is calculated as

$$s = s_0\left(1-\frac{c_{bs} b(\upsilon^*,\varepsilon)\alpha_c}{4\sqrt{\varepsilon}}\right), \quad (4)$$

where the multiplier C_{bs} is adjusted to account for the uncertainty of the bootstrap current effect.

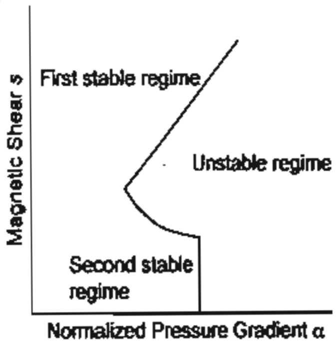

Fig. 1: The normalized pressure gradient vs. magnetic shear diagram (s-α diagram) is plotted. First and second stability region and unstable region is also described.

3. Results and Discussions

Statistical comparisons between predicted pedestal parameters and corresponding experimental values obtained from the ITPA Pedestal Database [10] version 3.2 are carried out. To quantify the comparison between the predictions of each model and experimental data, the root mean-square error (RMSE), the offset, and the Pearson product moment correlation coefficient (R) are computed. The RMSE, offset, and correlation R are defined as

$$\text{RMSE}\ (\%) = 100 \times \sqrt{\frac{1}{N}\sum_{j=1}^{N}\left[\ln\left(T_j^{\exp}\right) - \ln\left(T_j^{\text{mod}}\right)\right]^2}\ ,$$

$$\text{Offset}(\%) = \frac{100}{N}\sum_{j=1}^{N}\left[\ln\left(T_j^{\exp}\right) - \ln\left(T_j^{\text{mod}}\right)\right],$$

$$R = \frac{\sum_{j=1}^{N}\left(\ln\left(T_j^{\exp}\right) - \overline{\ln\left(T_j^{\exp}\right)}\right)\left(\ln\left(T_j^{\text{mod}}\right) - \overline{\ln\left(T_j^{\text{mod}}\right)}\right)}{\sqrt{\sum_{j=1}^{N}\left(\ln\left(T_j^{\exp}\right) - \overline{\ln\left(T_j^{\exp}\right)}\right)^2\left(\ln\left(T_j^{\text{mod}}\right) - \overline{\ln\left(T_j^{\text{mod}}\right)}\right)^2}}$$

where N is total number of data points, and $T_j^{\exp}$ and T_j^{mod} are the j^{th} experimental and model results for the temperature.

Six scalings for the pedestal temperature are derived using the six models described above for the width of the pedestal together with the model given by Eqs. (2) and (3) for the critical pressure gradient that includes both the first and second stability of ballooning modes. The pedestal temperature scalings are calibrated using 457 experimental data points (90 from JET experiment, and 367 from JT-60U experiment) for the ion pedestal temperature from the ITPA Pedestal Database (Version 3.2). The statistical results are shown in Table 1. The value of the coefficient, C_w, used in each of the expressions for the pedestal width and the value of multiplier C_{bs} used in the calculation of magnetic shear are given in the second and third column of Table 1, respectively. It is found that the RMSEs for the pedestal temperature range from 28.2% to 109.4%, where the model based on $\Delta \propto \rho s^2$ yields the lowest RMSE. For the offset, it is shown in Table 1 that the offsets range from -6.5% to 9.0%, where the model based on $\Delta \propto \rho s^2$ yields the best agreement (smallest absolute value of the offset). For the correlation R, it is shown in Table 1 that the values of correlation R range from 0.28 to 0.80, where the model based on $\Delta \propto \rho s^2$ yields the best agreement (highest value of R). From these results, it can be concluded that the pedestal temperature based on $\Delta \propto \rho s^2$ yields the best average agreement with experimental data.

Table 1: Statistical results of the models for type I ELMy H-mode discharges.

Pedestal width scaling	C_w	C_{bs}	RMSE (%)	Offset (%)	R
$\Delta \propto \rho s^2$	5.10	3.0	28.2	0.5	0.80
$\Delta \propto (\rho R q)^{1/2}$	0.22	4.5	35.4	2.9	0.75
$\Delta \propto R(\beta_{\theta,\text{ped}})^{1/2}$	1.50	3.7	35.5	-1.0	0.73
$\Delta \propto \rho^{2/3} R^{1/3}$	1.37	4.9	49.3	-1.1	0.67
$\Delta \propto \varepsilon^{1/2} \rho_\theta$	2.75	4.9	109.4	9.0	0.28
$\Delta \propto (1/Z)(A_H/n_{\text{ped}})^{1/2}$	0.014	5.9	50.5	-6.5	0.68

The comparisons between the predictions of the models and experimental data are shown in Figs. 2-7. It can be seen that the predictions of pedestal temperature are in reasonable agreement with experimental data for the model with $\Delta\propto\rho s^2$ shown in Fig. 2 and the agreement is not as good for the other models shown in Figs. 3-7.

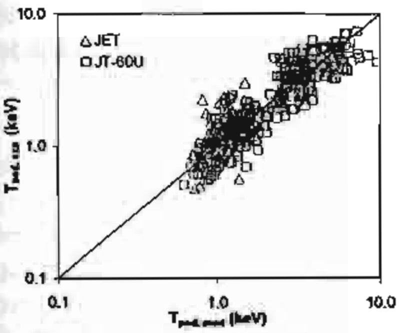

Fig. 2: Experimental ion pedestal temperature for type I H-mode plasmas compared with the model predictions based on $\Delta\propto\rho s^2$.

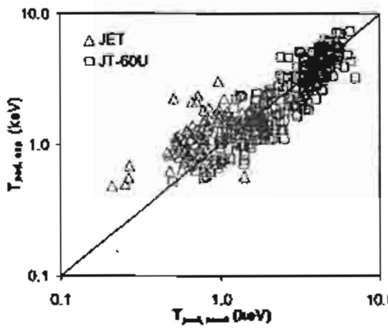

Fig. 3: Experimental ion pedestal temperature for type I H-mode plasmas compared with the model predictions based on $\Delta\propto(\rho Rq)^{1/2}$.

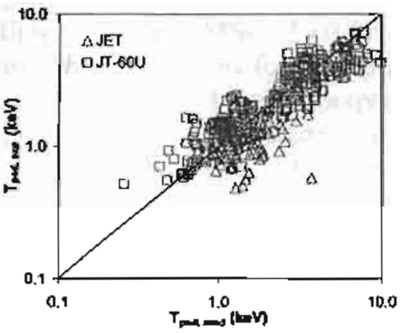

Fig. 4: Experimental ion pedestal temperature for type I H-mode plasmas compared with the model predictions based on $\Delta\propto R(\beta_{\theta,\mathrm{ped}})^{1/2}$.

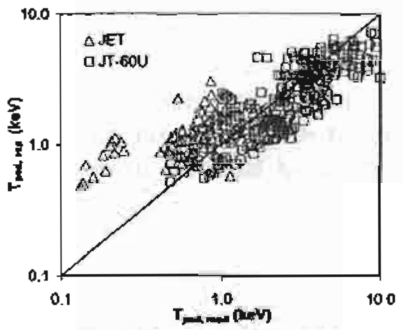

Fig. 5: Experimental ion pedestal temperature for type I H-mode plasmas compared with the model predictions based on $\Delta\propto\rho^{2/3}R^{1/3}$.

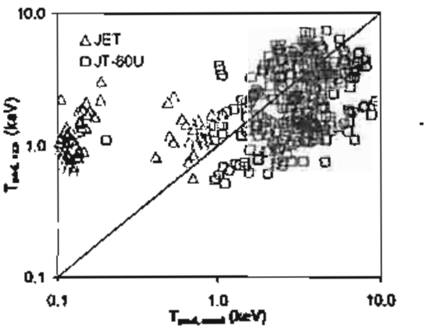

Fig. 6: Experimental ion pedestal temperature for type I H-mode plasmas compared with the model predictions based on $\Delta\propto\varepsilon^{1/2}\rho_\theta$.

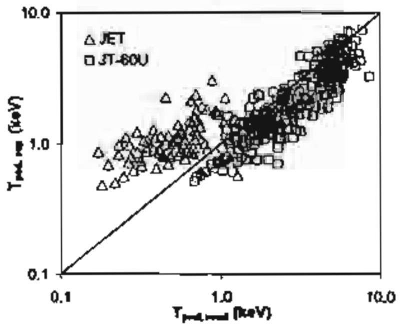

Fig. 7: Experimental ion pedestal temperature for type I H-mode plasmas compared with the model predictions based on $\Delta\propto(1/Z)(A_H/n_{\mathrm{ped}})^{1/2}$.

4. H-Mode Pedestal Density Model

In the development of the pedestal density model, an empirical approach is employed. For the simplest scaling, the pedestal density is assumed to be a function of line average density (n_l). This assumption is based on an observation that the density profile between the pedestal and the magnetic axis in H-mode discharges is usually rather flat. Therefore, the pedestal density is a large fraction of the line average density. It is found that the pedestal density scaling for type I ELMy H-mode discharges is about 72% of the line average density, which can be described as

$$n_{\rm ped} = 0.72 n_l . \tag{5}$$

This scaling yields an RMSE of 12.2%, R^2 of 0.96, and offset of -2.2% with a data set of 626 data points (132 from ASDEX-U experiment, 127 from JET experiment, and 367 from JT-60U experiment). In Ref. [11], a pedestal density scaling is developed for Alcator CMOD H-mode discharges. This scaling is expressed as a function of the line average density, plasma current (I_p), and toroidal magnetic field (B_T). Using this kind of power law regression fit for the 626 data points in the ITPA Pedestal Database (Version 3.2), the best predictive pedestal density scaling for type I ELMy H-mode discharges is found to be

$$n_{\rm ped}\left[10^{20}\,{\rm m}^{-3}\right] = 0.74\left(n_l\left[10^{20}\,{\rm m}^{-3}\right]\right)^{0.99}\left(I_p[MA]\right)^{0.15}\left(B_T[T]\right)^{-0.12} . \tag{6}$$

This scaling yields an RMSE of 10.9%, R^2 of 0.97, and offset of 3.3%. The comparisons of the density models' predictions for the pedestal density using Eq. (5) and (6) and the experimental data are shown in Figs. 8 and 9, respectively. In both figures, the agreement is good for a low ratio of pedestal density to the Greenwald density. However, the agreement tends to break away at high density. This might indicate that the physics that controls low and high edge density might be different.

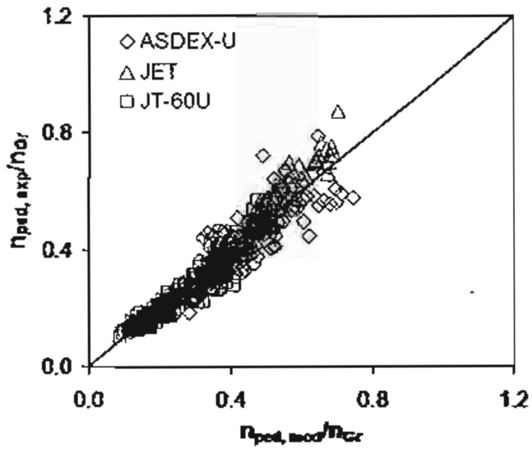

Fig. 8: The ratios of experimental pedestal electron density for type I H-mode plasmas to the Greenwald density are compared with the ratio of the model predictions using Eq. (5) to the Greenwald density.

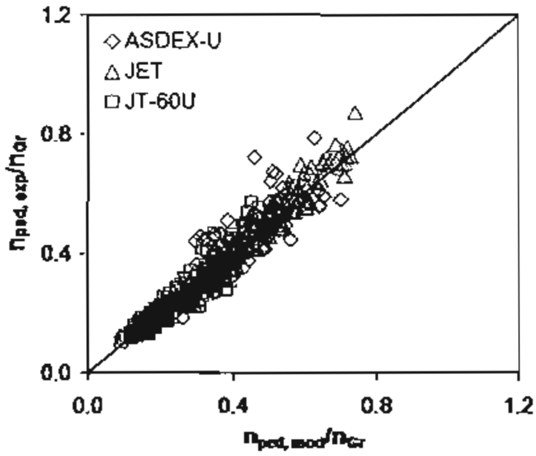

Fig. 9: The ratios of experimental pedestal electron density for type I H-mode plasmas to the Greenwald density are compared with the ratio of the model predictions using Eq. (6) to the Greenwald density.

5. Pedestal Prediction in ITER

The pedestal temperature and density models developed in this paper are used to predict the pedestal parameters for the ITER design. For an ITER standard H-mode discharge with 15 MA plasma current and the line average density of 1.05×10^{20} particles/m^3, the pedestal density is predicted to be 0.76×10^{20} particles/m^3 and 0.95×10^{20} particles/m^3 using Eqs. (5) and (6), respectively. It is worth noting that the pedestal density using Eq.(6) indicate a flat density profile since the pedestal density is almost the same as the line average density. This observation is often observed in H-mode experiments with high density. In addition, the pedestal density in ITER predicted using an integrated modeling code JETTO yields similar result for the density profile [12]. The pedestal temperature model based on the width of the pedestal as $\Delta \propto \rho s^2$ and the critical pressure gradient model that includes both first and second stability of ballooning modes is used to predict the pedestal temperature in ITER. Figure 10 shows the predicted pedestal temperature as a function of pedestal density. It can be seen that the pedestal temperature decreases as the pedestal density increases. At the predicted pedestal density using Eqs. (5) and (6), the predicted pedestal temperature is 1.9 and 1.7, respectively. Under these conditions, it is found that the pedestal width in ITER predicted by the model ranges from 4 to 5 cm.

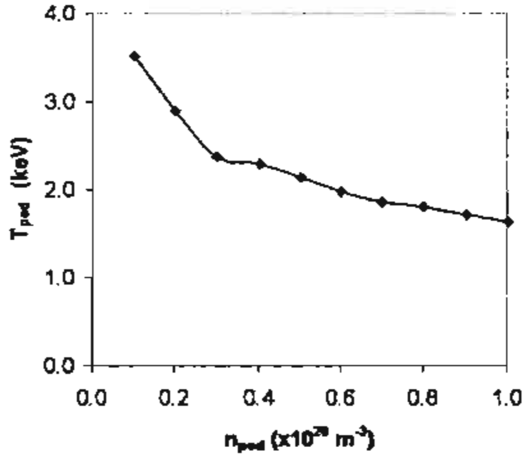

Fig. 10: Predictions of pedestal temperature as a function of pedestal density using the pedestal temperature model based on $\Delta \propto \rho s^2$

6. Conclusions

Pedestal temperature models that include the effects of both the first and second stability of ballooning modes are developed for type I ELMy H-mode plasmas in tokamaks. The results for the pedestal temperature are compared with experimental data obtained from the ITPA Pedestal Database version 3.2. It is found that the pedestal temperature model based on the magnetic and flow shear stabilization yields the best agreement with experimental data (with RMSE of 28.2%). It is found that the predictions of pedestal temperatures for ITER using the pedestal temperature and density models developed ranges from 1.7 to 1.9 keV.

4. Acknowleagement

Authors are grateful to Prof. Suthat Yoksan for his helpful discussions and to the ITPA Pedestal Database group for the pedestal data used in this work. This work is partially supported by Commission on Higher Education and the Thailand Research Fund (TRF) under Contract No. MRG4880165.

5. Referecnes

[1] Kinsey J E *et al.*, 2003 *Nucl. Fusion* **43** 1845
[2] Aymar R *et al.*, 2002 *Plasma Phys. Control. Fusion* **44** 519
[3] Onjun T *et al.*, 2002 *Phys. Plasmas* **9** 5018
[4] M Sugihara *et al.*, 2000 *Nucl. Fusion* **40** 1743
[5] T H Osborne *et al.*, 1999 *J. Nucl. Mater.* **266–269** 131
[6] B N Rogers *et al.*, 1999 *Phys. Plasmas* **6** 2797
[7] K C Shaing, 1992 *Phys. Fluids B* 4 290
[8] Guzdar P N *et al.*, 2005 *Physics of Plasmas* **12** 032502
[9] Onjun T *et al.*, 2004 *Phys. Plasmas* **11** 3006
[10] Hatae T *et al.*, 2001 *Nucl. Fusion* **41** 285
[11] Hughes J W *et al.*, 2002 *Physics of Plasmas* **9** 3019
[12] Onjun T *et al.*, 2005 *Physics of Plasmas* **12** 082513

บทความทางวิชาการตีพิมพ์ใน Proceeding ในการประชุมวิชาการระดับชาติ

The 2006 Siam Physics Congress ได้ตีพิมพ์ใน Thai Journal of Physics:

T. Onjun, A.H. Kritz, G. Bateman, and A.Y. Pankin, “Theoretical Predictions of Pedestal Temperature in ITER,” Thai Journal of Physics SERIES2 (2007) 12-17

Thai Journal of Physics SERIES 2 (2007) 12 – 17

SPC2006
Bangsaen

THEORETICAL PREDICTIONS OF PEDESTAL TEMPERATURE IN ITER

T. Onjun[1*], A. H. Kritz[2], G. Bateman[2] and A. Y. Pankin[3]

[1] *Department of Common and Graduate Studies, Sirindhorn International Institute of Technology, Thammasat University, Pathumthani 12121, Thailand*
[2] *Physics Department, Lehigh University, Bethlehem, PA 18015, USA*
[3] *SAIC, San Diego, CA 92121, USA*

Abstract

Models for the prediction of pedestal temperatures at the edge of type I ELMy H-mode plasmas are developed. These models are based on theory motivated concepts for pedestal width and pressure gradient. The pedestal pressure gradient is assumed to be limited by high-*n* ballooning mode instabilities, where both the first and second stability limits are considered. The effect of the bootstrap current, which reduces the magnetic shear in the steep pressure gradient region at the edge of the H-mode plasma, can result in access to the second stability of ballooning mode. In these pedestal models, the magnetic shear and safety factor are calculated at one pedestal width away from separatrix. The predictions of these models are compared with the high resolution pedestal data for type I ELMy H-mode discharges obtained from the latest public version (version 3.2) in the International Tokamak Physics Activity Edge (ITPA) Pedestal Database. The predictions of pedestal temperatures for ITER using these models are carried out. It is found that, at the design point, the pedestal temperature of ITER ranges from 2 to 4 keV, depending on the value of the pedestal density.

1. INTRODUCTION

It is well known that when the plasma heating power increases, plasmas can undergo a spontaneous self-organizing transition from a low confinement mode (L-mode) to a high confinement mode (H-mode) [1]. This plasma activity is widely believed to be caused by the generation of a flow shear at the edge of plasma, which is responsible for suppressing fluctuations and consequently transport near the edge of the plasma [2]. The reduction of the transport near the edge of the plasma results in a narrow sharply-defined region at the edge of plasma with steep temperature and density gradients, called the pedestal. This pedestal typically extends over with a width of about 5% of the plasma minor radius [3]. It was found that energy confinement in the H-mode regime of tokamaks strongly depends on the temperature and density at the top of the pedestal [4]. Therefore, it is important in the H-mode tokamak plasma studies, especially for the burning plasma experiment such as the "International Tokamak Experiment Reactor(ITER) [5]", to have a reliable prediction of the values at the top of the pedestal.

In the previous pedestal study by T. Onjun and colleagues in Ref. [6], six ranges of theoretical-based pedestal temperature models were developed utilizing six theoretical pedestal width models and the first stability ballooning mode pressure gradient limit. These pedestal temperature models also include geometrical effect, bootstrap current effect and separatrix effect, leading to complicated nonlinear behaviour. One weakness of these pedestal models is the assumption of the pressure gradient that plasma is in first stability regime of ballooning modes.

In this study, three pedestal temperature models in Refs. [6] are selected and extended to include effect of second stability limits of ballooning modes. The predictions from these modified pedestal temperature models will be tested against the latest public version of the pedestal data (Version 3.2) obtained from the International Tokamak Physics Activity (ITPA) Pedestal Database [7].

The paper is organized as follow. An expression for the H-mode pedestal temperature is described in Section 2. In Section 3, the predictions of the pedestal temperature resulting from the used of the model are compared with pedestal temperature data. A simple statistical analysis is used to characterize the agreement of the predictions of each model with

* Corresponding author . E-mail: thawatchai@siit.tu.ac.th

experimental data. In addition, the prediction of ITER is discussed. In Section 4, conclusions are presented.

2. H-MODE PEDESTAL MODELING

In the development of the pedestal temperature models, two ingredients are required — pedestal width (Δ) and pressure gradient ($\partial p/\partial r$) — while the pedestal density (n_{ped}) is obtained directly from the experiment. The temperature at the top of the pedestal (T_{ped}) can be estimated as

$$T_{ped} = \frac{1}{2 n_{ped} k} \left| \frac{\partial p}{\partial r} \right| \Delta \qquad (1)$$

where k is the Boltzmann constant. Note, the notation and units used in this paper are described in Table 1. One can obtain the value of T_{ped} giving the value of the pressure gradient in the pedestal region and the width of the pedestal region.

Table 1. Notation used in this paper.

Symbol	Unit	Physical description
R	m	Major radius to geometrical center of each flux surface
a	m	Plasma minor radius
I_p	MA	Plasma current
B_T	T	Vacuum toroidal magnetic field at R
A_H	amu	Hydrogenic mass
T_{ped}	keV	Pedestal temperature
n_{ped}	m^{-3}	Pedestal density
n_{Gr}	m^{-3}	Greenwald density $\left(I[MA]10^{20}/\pi a^2\right)$
q		Safety factor
ρ_i	m	Ion gyro rarius $\left(= 4.57\times10^{-3}\sqrt{\frac{A_H T}{B_T}}\right)$
$\beta_{\theta,ped}$		Normalized poloidal pressure in the pedestal $\left(\frac{4\mu_0 n_{ped} k T_{ped}}{\langle B_\theta\rangle^2}\right)$
$\langle B_\theta \rangle$	T	Average poloidal field around flux surface $\left(\approx \frac{\mu_0 I_p}{\pi a(1+\kappa)}\right)$
μ_0	Hm^{-1}	Permeability of free space
Z_{eff}		Effective charge
P_{aux}	MW	Auxiliary heating power

2.1 Scaling of pedestal width

Three theory-motivated models for the width of the pedestal are employed in this study. The brief details of these models are described in this section. These pedestal width models will be used together with the pedestal pressure gradient model to develop the pedestal temperature models.

2.1.1 Width scaling based on flow shear stabilization

In this model, the $E_r xB$ suppression of long wavelength modes is assumed to be the relevant factor in establishing the edge transport barrier [6]. The scaling of the pedestal width is found to be:

$$\Delta \propto \sqrt{\rho_i R q}\ , \qquad (2)$$

where ρ_i is the ion gyro radius, R is the major radius and q is the safety factor.

2.1.2 Width scaling based on magnetic and flow shear stabilization

The basic assumption of this model is that the transport barrier is formed in the region where the turbulence growth rate is balanced by a stabilizing $E_r xB$ shearing rate [8]. The scaling of the pedestal width is found to be:

$$\Delta \propto \rho_i s^2\ , \qquad (3)$$

where s is the magnetic shear.

2.1.3 Width scaling based on normalized poloidal pressure

In this model, the scaling of pedestal width is based on a model proposed by Osborne [9]. The scaling of the pedestal width is found to be:

$$\Delta \propto \sqrt{\beta_{\theta,ped}}R\ , \qquad (4)$$

where $\beta_{\theta,ped}$ is the normalized poloidal pressure.

2.2 Scaling of pressure gradient

In determining the pressure gradient inside the pedestal region for the type I ELMy H-mode discharges, it is assumed that the pressure gradient is limited by high-n ballooning mode instability in the short toroidal wavelength limit [10]. Recognizing that the pressure gradient in the pedestal region may depend on parameters such as magnetic shear (s), elongation (κ), and triangularity (δ), the pedestal pressure gradient can be estimated as:

$$\frac{\partial p}{\partial r} \approx \left(\frac{\partial p}{\partial r}\right)_c = -\frac{B_T^2 \alpha_c(s,\kappa,\delta)}{2\mu_0 R q^2}, \quad (5)$$

where α_c is the normalized critical pressure gradient of ballooning modes.

The ballooning mode is usually described using the magnetic shear vs. normalized pressure gradient diagram (s-α diagram) [11]. Normally, the calculation of ballooning mode stability is complicated, requiring information about the plasma equilibrium and geometry. A number of different codes have been developed for stability analysis, such as HELENA, MISHKA, and ELITE. In literature, several models for α_c were proposed. For example in Ref. [6], a scaling of α_c was proposed by assuming the restriction to first stability limit of ballooning modes and neglecting the second stability of ballooning modes, as

$$\alpha_c = 0.4s\left[1+\kappa_{95}^2\left(1+5\delta_{95}^2\right)\right] \quad (6)$$

where κ_{95} and δ_{95} are the elongation and triangularity at the 95% flux surface, respectively.

It has been widely observed in a number of experiments that the pedestal can obtain access to second stability limit of ballooning mode, especially in high triangularity discharges [12-14]. In Ref. [15], a simple scaling of α_c was proposed with the combination of first and second stability of ballooning modes. It was found that those scalings yield an improvement in the agreement with experimental data. In this paper, the scaling of α_c is proposed with the effect of first and second stability of ballooning modes included based on the stability analyses for several JET H-mode discharges carried out using the HELENA and MISHKA [16-18] . The stability analysis results suggest a simple form for the s-α MHD stability diagram as shown in Fig. 1, which leads to an analytic expression for α_c that includes the effect of both first and second stability of ballooning modes and the geometrical effect given by:

$$\alpha_c = C_0 \alpha_0(s)\left(\frac{1+\kappa_{95}^2\left(1+5\delta_{95}^2\right)}{2}\right) \quad (7)$$

where C_0 is a constant and

$$\alpha_0(s) = \begin{cases} 3+0.8(s-4) & ;s>4 \\ 5-2\sqrt{1-\left(\frac{4-s}{2}\right)^2} & ;4 \geq s \geq 2 \\ 2.5s & ;s<2 \end{cases}. \quad (8)$$

The numerical coefficients used in Eq. (8) are chosen according to the stability results of JET trangularity scan computed using the HELENA and MISHKA codes [16]. It is worth noting that, for $s > 4$, Eq. (8) indicates that the pedestal is in the first stability regime of ballooning modes. The scaling is similar to that proposed in Ref. [6]. For $4 \geq s \geq 2$, the scaling in Eq. (8) represents the regime of a transition from first to second stability of ballooning modes. For $s < 2$, the scaling in Eq. (8) represents a plasma that is in the second stability of ballooning modes, where the pedestal pressure gradient is limited by finite n ballooning mode stability. In Eq. (8), the bootstrap current and separatrix effects are also included through the calculation of magnetic shear. The details of the magnetic shear calculation is discussed in Ref. [6]. It is also noted that the effect of the current-driven peeling mode is not considered in this work.

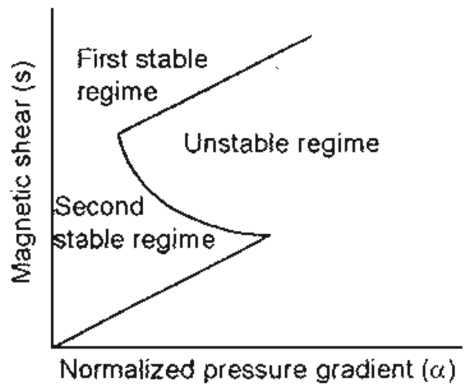

Fig. 1. The normalized pressure gradient vs. magnetic shear diagram (s-α diagram) is plotted. First and second stability region and unstable region is also described.

3. RESULTS AND DISCUSSION

Statistical comparisons between predicted pedestal parameters and corresponding experimental values obtained from the ITPA Pedestal Database [11] version 3.2 are summarized in terms of the RMSE presented in Table 2. The comparison is carried out for the high resolution pedestal data, which consist of 124 data points for the electron pedestal temperature, pedestal width, and pedestal pressure gradient. Note that the definitions of RMSE can be found in Ref. [6]. Results are presented for three pedestal temperature models. These three pedestal temperature models are based on three different models for the pedestal width along with the pressure gradient model for both first and second stability of ballooning modes, where the maximum normalized pressure gradient, α_c, is estimated using Eqs. (7) and (8). The value of the coefficient, C_w, used in each of the expressions for the pedestal width is given in the second column of Table 2. The value of the coefficient, C_0, used in each of the expressions for the pedestal normalized pressure gradient is given in the third column of Table 2. The values of C_w and C_0 were computed by minimizing the sum RMSE_T_{ped} + RMSE_Δ + RMSE_dp/dr. It is worth noting that the values of T_{ped} appears on both the left and right sides and is nonlinear in T_{ped} since q, α_c, and s are functions of position in the pedestal and, as a result, nonlinear functions of T_{ped}. The details of this nonlinear behavior are discussed in Ref. [6]. Thus, an iterative procedure is used in this paper to determine the temperature at the top of the pedestal.

It is found that the RMSEs for electron pedestal temperature (RMSE_T_{ped}) range from 57% to 63%. For the pedestal width, the RMSEs (RMSE_Δ) range from 30% to 38%. For the pedestal pressure gradient, the RMSEs (RMSE_dp/dr) range from 51% to 56%. All three models yield similar results for the comparison with experiment data.

The comparisons between the predictions of the model based on $\Delta\propto\rho s^2$ and experimental data are shown in Fig. 2 for the pedestal temperature (top panel), the pedestal width (middle panel), and the pressure gradient (bottom panel). It can be seen that the predictions of pedestal temperature, width and pressure gradient, are in reasonable agreement with experimental data.

Table 2: Coefficients and RMSEs of the models using the normalized pressure gradient model including both first and second stability limits of ballooning modes.

Width scaling	C_w	C_0	RMSE (%)		
			T_{ped}	Δ	dp/dr
$\Delta\propto(\rho Rq)^{1/2}$	0.10	0.8	60	32	56
$\Delta\propto\rho s^2$	0.29	0.8	63	38	51
$\Delta\propto(\beta_{\theta,ped})^{1/2}$	0.012	0.8	57	30	54

It is worth showing the improvement of the new pedestal models compared with the previous version of the pedestal models derived in Ref. [6]. Similar comparisons were carried in Ref. [6] using a different database of experimental measurements. Statistical comparisons of the predicted pedestal temperature, pedestal width, and pedestal pressure gradient with experimental data from the new database are shown in Table 3. It can be seen that RMSE_T_{ped} in Tables 2 and 3 are almost the same for all three models, but the values of RMSE_Δ and RMSE_dp/dr are significantly different.

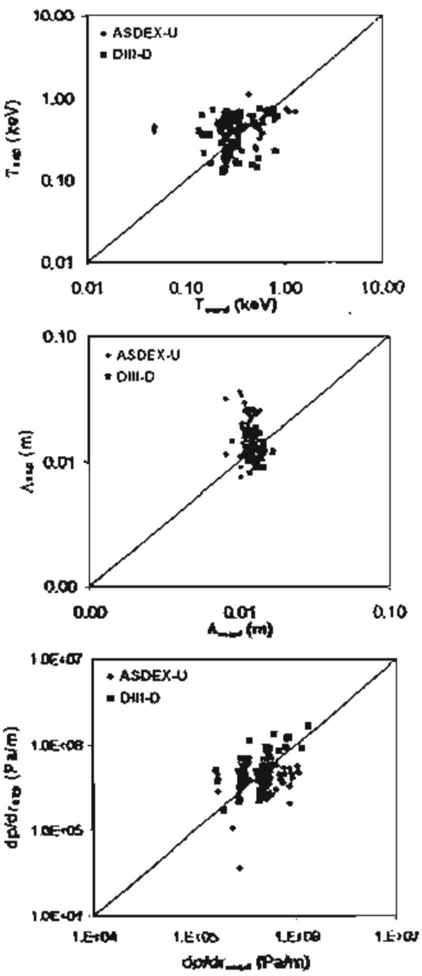

Fig. 2. Plot for the pedestal temperature (top), width (middle), and pressure gradient (bottom) predicted by model based on $\Delta\propto\rho s^2$ and the pedestal pressure gradient including both first and second stability of ballooning mode compared with experimental data from 124 data points. Each tokamak is indicated by a different symbol.

The effect of using a new pressure gradient model that includes second stability [Eqs. (7) and (8)] can be illustrated by deriving corresponding pedestal models using only the first stability condition [Eq. (6)]. The comparisons between the predictions of the model based on $\Delta \propto \rho s^2$ together with Eq. (6) and experimental data are shown in Fig. 3 for the pedestal temperature (top panel), the pedestal width (middle panel), and the pedestal pressure gradient (bottom panel). It can be seen that the predictions of pedestal temperature are in a reasonable range of experiment, while the pedestal widths are over-predicted and the pressure gradients are under-predicted relative to the data on the average. It can be concluded that the exclusion of access to second stability of ballooning mode results in the under-prediction of the pedestal pressure gradient in most of the discharges. In compensation for the under-prediction of the pedestal

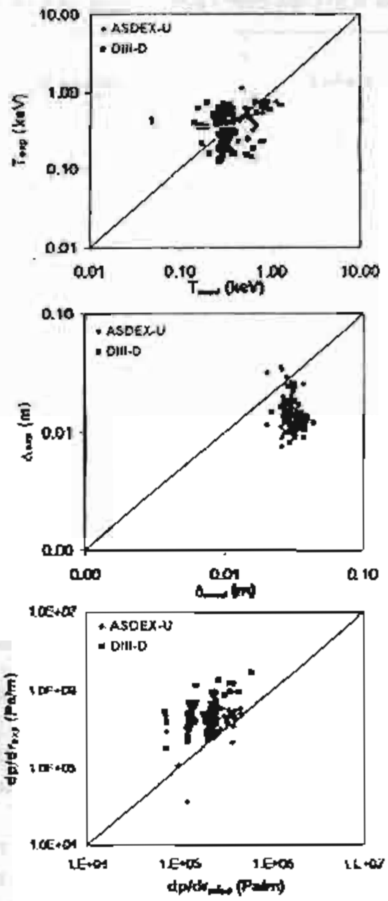

Fig. 3. Plot for the pedestal temperature (top), width (middle), and pressure gradient (bottom) predicted by model based on $\Delta \propto \rho s^2$ and the pedestal pressure gradient including only first stability compared with experimental data from 124 data points. Each tokamak is indicated by a different symbol.

Table 3: Coefficients and RMSEs of the models using the normalized pressure gradient model including only first stability limits of ballooning modes.

Width scaling	C_w	C_0	RMSE (%)		
			T_{ped}	Δ	dp/dr
$\Delta \propto (\rho R q)^{1/2}$	0.22	1.0	57	76	95
$\Delta \propto \rho s^2$	2.41	1.0	64	87	96
$\Delta \propto (\beta_{\theta,ped})^{1/2}$	0.021	1.0	62	43	81

pressure gradient, the prediction of the width is over-predicted on the average it in order to maximize agreement with the pedestal temperature.

Finally, the pedestal temperature models developed in this paper are used to predict the pedestal temperatures for the ITER design. Fig. 4 shows the predicted pedestal temperature as a function of the ratio of the pedestal density to the Greenwald density (n_{ped}/n_{gr}). It can be seen that the pedestal temperature decreases as the pedestal density increases. This trend has been observed in number of H-mode experiments [13]. At the design point, the line average density of ITER is 1.05×10^{20} m^{-3}. If assuming that the density profile is flat between the magnetic axis and the top of the pedestal, the pedestal density is approximately the same as the line average density. Thus, the ratio of the pedestal density to the Greenwald density in ITER is equal to 0.84 and, consequently, the pedestal electron temperature is predicted to ranges from 2.3 to 2.7 keV. Note that the ITER simulation using the JETTO code in Ref. [19] indicates that the ITER density profile is flat. The "design point" would shift to the left in Fig. 4 and, consequently, to a higher pedestal temperature, if the pedestal density were taken to be less than the line average density. For example, in Ref. [20], the pedestal density for type I ELMy H-mode plasmas is found to be 71% of the line average density. Thus, according to this model, the pedestal density for ITER is 7.5×10^{19} m^{-3} (n_{ped}/n_{gr} =0.62). Therefore, the pedestal temperature ranges from 2.9 to 3.7 keV.

It is also found that the pedestal width in ITER is predicted by all three models to be about 3 cm. Because of the narrow pedestal width, it is not surprising to obtain relatively low values for the pedestal temperature in ITER. It was reported in Ref. [19] that with the width of 3 cm, the JETTO simulation yields the pedestal electron temperature of 2.3 keV, which is in the range of the result obtained in this paper.

4. CONCLUSION

Pedestal temperature models that include the effects of both first and second stability of ballooning

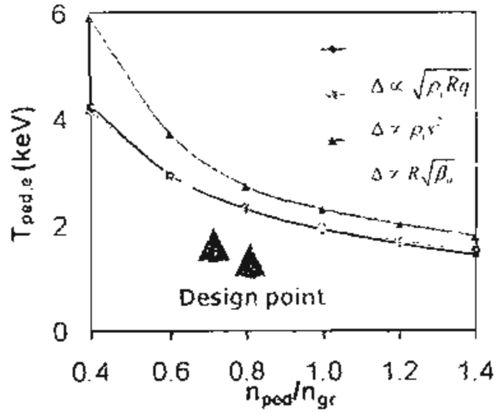

Fig 4. Predictions of pedestal temperature as a function of the pedestal density based on three pedestal temperature models.

Table 4: The basic parameters for ITER design

Parameters	Values
Major radius	6.2 *m*
Minor radius	2.0 *m*
Plasma current	15 MA
Toroidal magnetic field	5.3 T
Elongation	1.85
Triangularity	0.48
Line average density	$1.05\text{x}10^{20}\ m^{-3}$
Effective charge	1.4
Auxillary power	40 MW

modes are developed for type I ELMy H-mode plasmas in tokamaks. The results for the pedestal temperature, width and pressure gradient are compared with high resolution data points in the ITPA Pedestal Database version 3.2. It is found that the inclusion of the second stability of ballooning modes improves the agreement with experimental data for the pedestal pressure gradient and, consequently, for the width. The predictions of pedestal temperatures for ITER using these models are found that, at the design point, the pedestal temperature of ITER ranges from 2 to 4 keV, depending on the value of the pedestal density.

ACKNOWLEDGMENTS

T. Onjun is grateful to Prof. Suthat Yoksan for hishelpful discussions and also thanks the ITPA Pedestal Database group for the pedestal data used in this work. This work is supported by Commission on Higher Education and the Thailand Research Fund (TRF) under Contract No. MRG4880165.

REFERENCES

[1] F. Wagner, G. Becker, K. Behringer, *et al.*, Physical Review Letters, 49(19) (1982) 1408.
[2] K. H. Burrell, Physics of Plasmas, 4(5) (1997) 1499.
[3] A. E. Hubbard, Plasma Phys. Control. Fusion, 42 (2000) A15.
[4] J. E. Kinsey, G. Bateman, T. Onjun, *et al.*, Nuclear Fusion, 43 (2003) 1845.
[5] R. Aymar, P. Barabaschi, and Y. Shimomura (for the ITER team), Plasma Phys. Control. Fusion, 44 (2002) 519.
[6] T. Onjun, G. Bateman, A. H. Kritz, *et al.*, Physics of Plasmas, 9(12) (2002) 5018.
[7] T. Hatae, M. Sugihara, A. E. Hubbard, *et al.*, Nuclear Fusion, 41(3) (2001) 285.
[8] M. Sugihara, Yu. Igitkhanov, G. Janeschitz, *et al.*, Nuclear Fusion, 40(10) (2000) 1743.
[9] T. H. Osborne, K. H. Burrell, R. J. Groebner, *et al.*, Journal of Nuclear Materials, 266-269 (1999) 131.
[10] J. W. Connor, Plasma Phys. Control. Fusion, 40 (1998) 191.
[11] J. Wesson, *Tokamaks*. 2nd ed. Clarendon, Oxford, England. (1997).
[12] Y. Kamada, T. Hatae, T. Fukuda, *et al.*, Plasma Phys. Control. Fusion, 41 (1999) 1371.
[13] T. H. Osborne, J. R. Ferron, R. J. Groebner, *et al.*, Plasma Phys. Control. Fusion, 42 (2000) A175.
[14] W. Suttrop, O. Gruber, B. Kurzan, *et al.*, Plasma Phys. Control. Fusion, 42 (2000) A97.
[15] T. Onjun, Laser and Particle Beams, 24 (2006) 113.
[16] T. Onjun, A. H. Kritz, G. Bateman, *et al.*, Physics of Plasmas, 11(6), (2004) 3006.
[17] T. Onjun, A.H.K., G. Bateman, *et al.*, Physics of Plasmas, 11(4) (2004) 1469.
[18] J.-S. Lonnroth, V. V. Parail, G. Corrigan, *et al.*, Plasma Phys. Control. Fusion, 45 (2003) 1689.
[19] T. Onjun, A. H. Kritz, G. Bateman, *et al.*, Physics of Plasmas, 12(8), (2005) 082513.
[20] G. Bateman, T. Onjun, and A. H. Kritz, Plasma Phys. Control. Fusion, 45 (2003) 1939.

บทความทางวิชาการที่ส่งตีพิมพ์ใน Proceeding ในการประชุมวิชาการระดับชาติ

The 2007 Siam Physics Congress

SELF-CONSISTENT MODELING OF ITER WITH THE INTEGRATED PREDICTIVE MODELING CODE

Thawatchai Onjun[1*], Vassili Parail[2], Arnold H. Kritz[3], Glenn Bateman[3] and Alexei Y. Pankin[3]

[1]*Sirindhorn International Institute of Technology, Thammasat University, Klong Luang, Pathumthani, 12121, Thailand*

[2]*Euratom/UKAEA, Fusion Association, Culham Science Centre, Abingdon, OX14 3DB, UK*

[3]*Department of Physics, Lehigh University, Bethlehem, Pennsylvania, 18015, USA*

Abstract

Self-consistent modeling of the International Thermonuclear Experimental Reactor (ITER) has been carried out using integrated predictive modeling codes in which theory-based models are used for both core and edge transport. The model for the H-mode pedestal in tokamak plasmas is based on flow shear reduction of anomalous transport, while the periodic ELM crashes are triggered by MHD instabilities. Suppression of the anomalous transport enhances the role of neoclassical transport in the pedestal region. In the simulations, an ELM crash can be triggered either by a pressure-driven ballooning mode or by a current-driven peeling mode, depending on which instability reaches its stability criterion first. Performance of ITER in a standard Type I ELMy H-mode scenario with the designed parameters is found to be optimistic, in which BALDUR and JETTO simulations yield the fusion Q of 10.6 and 16.6, respectively. The difference is caused by the difference in pedestal predictions.

Keywords: Plasma; H-mode; ELMs; Pedestal; Modelling; ITER

1 INTRODUCTION

The International Thermonuclear Experimental Reactor (ITER) is an international collaborative effort with the aim to demonstrate the scientific and technological feasibility of fusion energy [1]. This is an important step for magnetic confinement fusion research. With a decision to construct the device in France, a big step forward has been taken to explore the properties of long burning plasma. It has been found in both theoretical and experimental work about the dependence of high confinement mode (H-mode) performance on the pedestal. In this paper, the performance of ITER is investigated using predictive integrated modeling codes. It is important to simulate ITER plasma and to predict the ITER performance in advance, which will lead to a way to improve the performance if needed and to have a better chance of success.

An objective of integrated modelling simulations is to predict the time evolution of the plasma temperature, density, and other profiles in tokamak plasmas. Large integrated modelling codes compute the sources, sinks, and transport of thermal energy and particle densities, as well as the equilibrium shape of the plasma and the effects of large-scale instabilities. A number of transport models have been developed for use in integrated modelling codes. The results of simulations using these integrated predictive modeling codes have been intensively compared with experimental data from a wide range of tokamak discharges.

Achieving the fusion ignition (at least fusion Q of 10) is one of goals in fusion study of ITER. As a result, burning plasma experiments such as ITER is designed to operate in the high mode (H-mode) regime. H-mode discharges in tokamaks generally provide excellent energy confinement and have acceptable particle transport rates for impurity control. However, H-mode discharges are often perturbed by quasi-periodic bursts of magnetohydrodynamics (MHD) activity at the edge of the plasma, which are known as edge-localized modes (ELMs). Each ELM crash results in a rapid loss of particles and energy from the edge of the plasma, which can reduce the average global energy content by 10%–20%. Furthermore, these transient bursts of energy and particles into the scrape-off layer produce high-peak heat loads on the divertor plates. On the other hand, the ELMs remove heat and particles, including impurities, from the region near the separatrix. ELMs also play an essential role in the control of the height of the H-mode pedestal, which is found to be important for obtaining ITER performance. In this paper, we summarize the ITER prediction using two different integrated predictive modeling codes, BALDUR [2] and JETTO [3].

A brief concept for integrated predictive modeling code is addressed in Sec.2. The ITER prediction using BALDUR integrated predictive modeling code is described in Sec. 3, while The ITER prediction using

JETTO integrated predictive modeling code is presented in Sec. 4. Conclusions are given in Sec. 5.

2 H-MODE PEDESTAL MODELING

A number of integrated predictive modeling codes, such as the BALDUR code, the JETTO code, the ASTRA code [4], the CORSICA code [5], the XPTOR code [6], the TSC code [7], the ONETWO code [8], and the CRONOS code [9], have been developed to carry out simulations in order to predict the time evolution of the tokamak plasma current, temperature, and density profiles. With the predicted profiles

One objective of these simulations is to develop a better understanding of the physical processes and the inter-relationships between those physical processes that occur in tokamak plasma experiments. The simple schedule explains about how it works is shown in figure 1. Basically, it is a collection of several modules, such as a neutral beam heating module, an RF heating module, core transport module, impurity radiation module, in which each module is responsible for different task. These modules are work together, which results in a complex scenario and similar to what occurs in real experiments. In general, the input data for integrated predictive modeling code is similar to controlled parameters in experiments, such as magnetic field, total heating power, and plasma current.

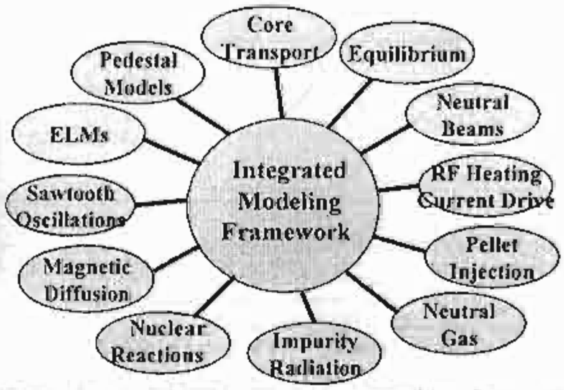

Figure 1: A simple scheme describes how an integrated predictive modeling code works.

3. ITER simulations using BALDUR code

The BALDUR integrated predictive modelling code is used to compute the time evolution of plasma profiles including electron and ion temperature, deuterium and tritium density, helium and impurity density, magnetic q, neutrals, and fast ions. These time-evolving profiles are computed in the BALDUR code by combining the effects of many physical processes self-consistently, including the effects of transport, plasma heating, particle influx, boundary conditions, the plasma equilibrium shape, and sawtooth oscillations. Fusion heating and helium ash accumulation are computed self-consistently.

The BALDUR integrated predictive modelling code contains a variety of modules for computing sources, sinks, transport, boundary conditions, and the effect of large-scale instabilities. For the simulations of burning plasma experiments presented in this paper, the core transport is calculated using MMM95 module [10] and the boundary is taken to be at the top of the pedestal. The temperature at boundary is calculated using the model based on magnetic and flow shear stability together with ballooning mode limit. This model can be expressed as:

$$T_{ped} = 1.89\left(\frac{B_T}{q^2}\right)^2\left(\frac{A_H}{R^2}\right)\left(\frac{\alpha_c}{n_{ped,19}}\right)^2 s^4 \qquad (1)$$

where T_{ped} is the pedestal height in units of keV, B_T is the magnetic field, q is the safety factor, A_H is the average hydrogenic ion mass, R is the major radius, αc is the normalized critical pressure gradient of the ballooning modes, $n_{ped,19}$ is the electron density at the top of the pedestal in units of 10^{19} m^{-3} and s is the magnetic shear. The detailed development of this model can be found in Ref. [11]. For the density at the top of the pedestal is calculated using the following formula:

$$n_{ped} = 0.71 n_l \qquad (2)$$

where n_{ped} is the pedestal density and n_l is the line average density. It is worth noting that the values at the top of the pedestal are crucial for the prediction since it was found in both experimental and theoretical work that the performance in H-mode depends sensitively on the pedestal height.

Table 1: The basic parameters for ITER design

Parameters	Values
Major radius	6.2 m
Minor radius	2.0 m
Plasma current	15 MA
Toroidal magnetic field	5.3 T
Auxillary power	40 MW

Simulation of ITER is carried using BALDUR integrated predictive modeling code with parameters described in Table 1. Figure 2 shows the temperature and density profiles as a function of major radius at the end of the ITER simulation at 300 s. The values of temperature and density at the edge of the simulation are given by the pedestal models. It is found that the pedestal temperature in ITER is close to 3 keV and the pedestal density is about 0.7×10^{20} m^{-3}. The steep gradient region of the H-mode pedestal lies outside the simulation. It can be seen in figure 2 that the density profile in ITER is relatively flat, with a small region with a relatively steep density gradient near the edge of the simulation. Also, it can be seen in figure 2 that the central electron and ion temperatures are about 20 keV, where the central electron temperature is somewhat higher than the central ion temperature due to the fact that the fast alpha particles produced by fusion reactions heat the electrons more than the ions.

Normally, the performance of fusion reaction can be calculated in term of fusion Q, which can be expressed as

$$\text{Fusion Q} = \frac{\text{Output energy}}{\text{Input energy}}. \qquad (4)$$

Based on these profiles from BALDUR predictions, the performance of ITER can be calculated. The total nuclear fusion power production of ITER is found to be close to 400 MW, which results in the fusion Q of 10.6.

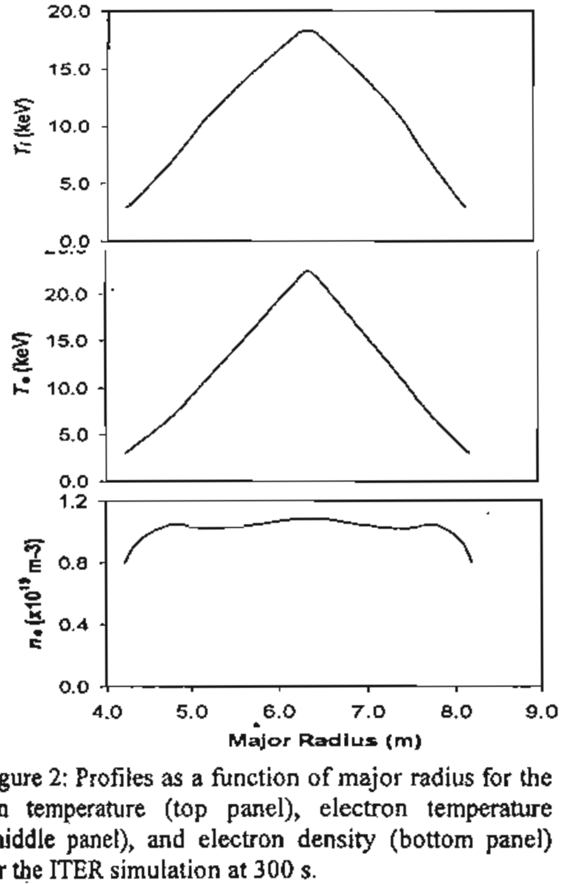

Figure 2: Profiles as a function of major radius for the ion temperature (top panel), electron temperature (middle panel), and electron density (bottom panel) for the ITER simulation at 300 s.

4. ITER simulations using JETTO code

The 1.5 D JETTO transport code is used to evolve the plasma current, temperatures, and density profiles throughout the plasma, including both the core and pedestal regions. The core transport is calculated using the mixed Bohm/gyro-Bohm model [12] together with the NCLASS neoclassical model [13]. For the pedestal region, two assumptions are applied in this work. One assumption is that of the pedestal width which is fixed equal to 6 cm. The second assumption is that the anomalous turbulent transport is completely suppressed by the flow shear in the region between the top of the pedestal and the separatrix, resulting in the establishment of a steep gradient region. In the pedestal region prior to an ELM crash, transport is computed by taking all the diagonal elements of the transport matrix within the pedestal equal to the ion neoclassical thermal conductivity, calculated at the top of the pedestal using NCLASS.

Figure 3 shows the temperature and density profiles as a function of minor radius at the time before an ELM crash of the ITER simulation when the profiles reach steady state. It can be seen the steep gradient region of the H-mode pedestal lies near the edge of the simulation, which is called the pedestal. It is also found that the temperature at the top of the pedestal in ITER is close to 5 keV and the density at the top of the pedestal is 1.0×10^{20} m^{-3}. It can be seen in figure 3 hat the density profile in ITER is relatively flat, with a small region with a relatively steep density gradient near the edge of the simulation. This observation is similar with the ITER prediction from BALDUR code. Also, it can be seen in figure 3that the central ion and electron temperatures are about 20 and 30 keV, respectively. Based on these profiles from JETTO predictions, the total nuclear fusion power production of ITER is found to be close to 700 MW, which results in the fusion Q of 16.6.

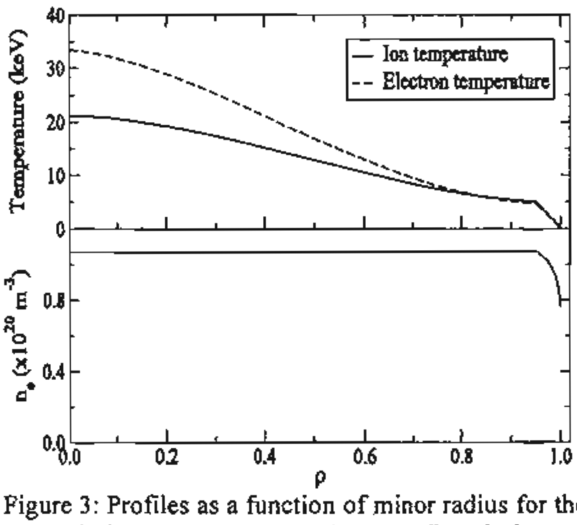

Figure 3: Profiles as a function of minor radius for the Ion and electron temperature (top panel) and electron density (bottom panel) for the ITER simulation before an ELM crash when the profiles reach steady state.

It can be seen that the fusion Q increases from 10.6 in BALDUR simulation to 16.6 in JETTO simulation. The nuclear power production increases more than 50%. This increase is mainly a result of higher pedestal value. In BALDUR code, the top of the pedestal temperature is found to be about 3 keV; whereas it is found to be about 5 keV in JETTO simulation. The higher pedestal value in JETTO simulation can be explained by access to second stability effect of ballooning mode, which did not include in BALDUR simulation.

5. Conclusions

Self-consistent simulations of ITER have been carried out using the BALDER and JETTO-integrated modeling codes in which theory-motivated models are used for both core and edge transport. The flat density and peak temperature profiles are found from both codes. It is found that the fusion performance, expressed in term of fusion Q, is found to be optimistic. The pedestal prediction plays important role in the predictions.

6. Acknowleagement

T. Onjun is grateful to Prof. Suthat Yoksan for his helpful discussions. This work is supported by Commission on Higher Education and the Thailand Research Fund (TRF) under Contract No. MRG4880165.

7. Referecnes

[1] R. Aymar, P. Barabaschi, and Y. Shimomura (for the ITER team), *The ITER design.* Plasma Phys. Control. Fusion, 2002. **44**: p. 519.

[2] C. E. Singer, D. E. Post, D. R. Mikkelsen, *et al.*, Baldur: A one-dimensional plasma transport code. Computer Physics Communications, 1988. **49**(2): p. 275.

[3] G. Cenacchi and A. Taroni, JETTO: A free-boundary plasma transport code. JET-IR (88), 1988.

[4] G. Pereverzev and P. N. Yushmanov, ASTRA Automated System for Transport Analysis in a Tokamak. Max-Planck Institut fur Plasmaphysik (IPP 5/98), 2002.

[5] L. D. Pearlstein, R. H. Bulmer, T. A. Casper, *et al.*, in Proceedings of the 28th EPS Conference on Controlled Fusion and Plasma Phys. 2002. Madeira, Portugal.

[6] J. E. Kinsey, G. M. Staebler, and R. E. Waltz, Simulations of internal transport barrier formation in tokamak discharges using the GLF23 transport model. Physics of Plasmas, 2002. **9**(5): p. 1676.

[7] S. C. Jardin, N. Pomphrey, and J. DeLucia, Dynamic modeling of transport and positional control of tokamaks. Journal of Computational Physics, 1986. 66(2): p. 481.

[8] W. W. Pfeiffer, F. B. Marcus, C. J. Armentrout, *et al.*, Giant sawtooth oscillations in the Doublet III tokamak. Nuclear Fusion, 1985. **25**: p. 655.

[9] V. Basiuk, J. F. Artaud, F. Imbeaux *et al.*, Simulations of steady-state scenarios for Tore Supra using the CRONOS code. Nuclear Fusion, 2003. **43**: p. 822.

[10] T.Onjun, A. H. Kritz, G. Bateman, *et al.*, *Integrated pedestal and core modeling of Joint European Torus (JET) triangularity scan discharges.* Physics of Plasmas, 2004. **11**(6): p. 3006.

[11] M. Erba, A. Cherubini, V. V. Parail, *et al.*, Development of a non-local model for tokamak heat transport in L-mode, H-mode and transient regimes. Plasma Phys. Control. Fusion, 1997. 39(2): p. 261.

[12] W. A. Houlberg, K. C. Shaing, S. P. Hirshman, *et al.*, Bootstrap current and neoclassical transport in tokamaks of arbitrary collisionality and aspect ratio. Physics of Plasmas, 1997. 4(9): p. 3230.